Engineered Science
DOI: https://dx.doi.org/10.30919/es1683

Review on Thermoelectric Aerogels and their Preparation Methods and Innovative Applications

Shuaimin Zheng,[1] Junting Lei,[1] Sri Hari Kumar Annamareddy,[2] Duo Pan,[1,*] Chuntai Liu,[1] Changyu Shen[1], Zhansaya Lakhbayeva[3] and Zhexenbek Toktarbay[3]

Abstract

Thermoelectric aerogel is a novel type of material that can achieve the interactive transformation between electrical energy and thermal energy. Due to its unique characteristics such as low density, low thermal conductivity, high elasticity, and excellent thermoelectric properties, now it has received extensive attention in different fields such as high-temperature energy harvesting, intelligent sensing, and self-powered systems. This paper reviews the working principle and latest research progress of thermoelectric aerogels, including structural design innovation, performance optimization, and expansion of application fields. It focuses on exploring the application potential of thermoelectric aerogels in wearable devices, high-temperature monitoring and early warning, energy harvesting and conversion, and looks forward to its future development directions.

Keywords: Thermoelectric aerogel; Thermoelectric principle; Structural design; Thermoelectric performance; Future prospect.
Received: 25 June 2025; Revised: 13 August 2025; Accepted: 19 August 2025.
Article type: Review article.

1. Introduction

With the rapid development of the Internet of Things, wearable electronics and intelligent equipment face unprecedented opportunities and challenges, imposing stringent requirements on power supply systems.[1-4] Traditional power supplies are limited in energy acquisition and stable operation, highlighting the urgency to develop efficient, self-powered energy conversion materials adaptable to complex environments.[5-9] Thermoelectric aerogel, as a highly promising new material, is gradually becoming a research hotspot.

Thermoelectric materials rely on the Seebeck effect and the Palladium effect to achieve direct interconversion of thermal and electrical energy.[10-14] Compared with other energy conversion technologies, thermoelectric generators exhibit remarkable technical characteristics: they are less affected by the intensity of solar radiation, operate without noise, low heat source requirements.[15] The core technical advantage lies in that the directional migration of carriers inside the material in a temperature gradient environment directly generates direct current.[16-19] This characteristic enables it to seamlessly adapt to the power supply requirements of electronic devices. Since the discovery of the thermoelectric effect in the 19th century, research on improving the thermoelectric performance of materials has been continuously progressing.[20-23] With the advancement of size effect theory, the technology for band structure regulation has been continuously optimized.[24-25] High performance thermoelectric materials have been widely applied in fields such as solid state refrigeration devices and deep space power generation equipment.[26] Driven by the systematic advancement of size effect theory, the technological maturity of band engineering, and the successful fabrication of novel functional materials, remarkable breakthroughs have been achieved in exploring high performance thermoelectric materials.[27-28]

Thermoelectric aerogels enable efficient conversion between thermal and electrical energy by virtue of their unique microstructures and material properties. Compared with conventional thermoelectric materials, thermoelectric aerogels offer prominent advantages: light weight, excellent flexibility to adapt to complex and changeable application

[1]*Key Laboratory of Materials Processing and Mold (Zhengzhou University), Ministry of Education, National Engineering Research Center for Advanced Polymer Processing Technology, Zhengzhou University, Zhengzhou, 450002, China*
[2]*Department of Chemical and Petrochemical Engineering, University of Nizwa, Birkat Al-Mouz, 616, Sultanate of Oman*
[3]*Department of Chemistry, Faculty of Natural Sciences and Geography, Abai Kazakh National Pedagogical University, 30, Kazybek bi, 05001, Almaty, Kazakhstan*
[*]*Email*: panduonerc@zzu.edu.cn (D. Pan)

scenarios, and good thermal insulation performance, maintaining stable internal conversion environments. Their key advantage lies in the synergistic effect of specially arranged nanostructures and conductive components within the aerogel, which promotes the efficient directional movement of charge carriers under temperature gradients, thereby stably generating direct current (DC). This feature allows them to be conveniently adapted to the needs of miniaturized and flexible power supplies for wearable electronic devices and other applications.[29-32] The thermoelectric performance of these materials essentially hinges on the dimensionless figure of merit (*ZT*).[33-34] Various thermoelectric aerogel s have been prepared using a variety of materials including polymers such as poly(3,4-ethylenedioxythiophene):poly(styrenesulfonate) (PEDOT:PSS), polyaniline (PANI),[35-36] and a number of insulating polymers (cellulose or polyurethanes), carbon-based materials such as graphene and carbon nanotubes,[37-38] as well as their composite and hybrid counterparts.[39-42] Using the compressibility, electrical conductivity, Seebeck effect, and excellent thermoelectric conversion ability of thermoelectric aerogels, they can be widely applied to piezoresistive pressure/strain sensors, temperature sensors, or thermoelectric generators.[43-47] To achieve these functional applications, temperature is a key parameter, which not only affects the thermoelectric properties of the aerogel itself but also determines its performance and practical applications as a sensor or generator.[48]

However, the development of thermoelectric aerogels still faces many challenges. In terms of material performance, how to further improve their thermoelectric conversion efficiency and enhance their mechanical stability and flexibility to meet the needs of different application scenarios remains an urgent problem to be solved. In terms of preparation processes, most of the current preparation methods have disadvantages such as high cost, complex processes, and difficulty in large-scale production, which limit the industrialization process of thermoelectric aerogels. In terms of system integration, effectively integrating thermoelectric aerogels with other functional materials or devices to achieve multifunctional integration is also one of the current research difficulties. Despite these challenges, with the continuous progress of materials science, nanotechnology, and manufacturing processes, the research and application prospects of thermoelectric aerogels are still broad. In depth research on the preparation methods, structural properties of thermoelectric aerogels, and their applications in various fields is of great practical significance for promoting the development of wearable electronic devices and intelligent protective equipment.

2. Basic thermoelectric principles

The core working mechanism of thermoelectric materials is based on the Seebeck effect and the Peltier effect (Fig. 1). The former enables the conversion of thermal energy into electrical energy, while the latter is the reverse process of converting electrical energy into thermal energy.[49] In the presence of a temperature gradient across a material, the Seebeck effect drives thermal excitation of carriers: holes in p-type semiconductors and electrons in n-type semiconductors migrate directionally, generating an electric current in the external circuit.[22] The Peltier effect, the inverse of the Seebeck effect, refers to heat transfer at material junctions driven by an electric current. This unique characteristic has been applied to advanced applications in solid-state refrigeration, enabling efficient thermal management technologies.[24]

The dimensionless figure of merit *ZT* is used to quantify the energy conversion efficiency of thermoelectric materials, which is expressed as Eq. (1):[50-51]

$$\mathrm{ZT} = \frac{S^2 \sigma T}{k} \tag{1}$$

where *S*, σ, *T*, and *k* represent the Seebeck coefficient, electrical conductivity, thermodynamic temperature in Kelvin scale, and thermal conductivity, respectively. To enhance the *ZT* value, a synergistic optimization of three key parameters is essential: elevating the Seebeck coefficient and electrical conductivity while reducing thermal conductivity. In thermoelectric materials, the three key parameters exhibit inherent coupling: increasing carrier concentration to boost electrical conductivity often compromises the Seebeck coefficient due to carrier energy filtering effects, thereby requiring sophisticated strategies such as band structure engineering and nanostructural design to achieve parameter decoupling.[52]

The thermoelectric power factor *PF* is composed of the electrical conductivity and the Seebeck coefficient, and its definition is Eq. (2):

$$PF = S^2 \tag{2}$$

The Seebeck coefficient is expressed by the following Eq. (3):[53-54]

$$\mathrm{S} = \frac{\pi^2 {K_\mathrm{B}}^2 T}{3q} \left\{ \frac{\mathrm{d}n(E)}{n\mathrm{d}E} + \frac{\mathrm{d}\mu(E)}{\mu \mathrm{d}E} \right\}_{E=E_\mathrm{F}} \tag{3}$$

where k_B is the Boltzmann constant, *q* is the carrier charge, $\mu(E)$ is the mobility, and $n(E)$ is the carrier density. This formula indicates that an ideal Seebeck coefficient can be obtained by increasing the dependence of the mobility and the carrier density on energy. In addition, for degenerate semiconductors, the Seebeck coefficient can be represented by a simplified formula that includes the carrier effective mass m^* as Eq. (4):[53-56]

$$\mathrm{S} = \frac{8\pi^2 {K_\mathrm{B}}^2 m^* T}{3qh^2} \left(\frac{\pi}{3n} \right)^{\frac{2}{3}} \tag{4}$$

There are two strategies to increase the effective mass m^*: one is to improve the symmetry of the crystal structure; the other feasible method is to increase the band effective mass through chemical doping, which helps to flatten the energy band and generate resonant energy levels.[13] Although the Seebeck coefficient is increased, a low carrier density will also

lead to a decrease in electrical conductivity. The definition of electrical conductivity σ is Eq. (5):[51]

$$\sigma = nq\mu \quad (5)$$

where n is the carrier density, q is the carrier charge, and μ represents the carrier mobility. As the carrier density increases, the Seebeck coefficient decreases and the electrical conductivity increases, which reflects the strong coupling relationship between the Seebeck coefficient and the electrical conductivity.[22,53] Therefore, the optimal power factor can be obtained by adjusting the carrier density.[57]

In thermoelectric materials, the heat conduction mechanism includes the transport of electrons and holes as well as the propagation of phonons related to the lattice thermal motion. In the case of single type carrier transport, the thermal conductivity can be expressed as the sum of the carrier thermal conductivity k_c and the lattice thermal conductivity k_l as: Eqs. (6) and (7).[58]

$$k = k_c + k_l \quad (6)$$

$$k_c = L_0 \sigma T = L_0 ne\mu T \quad (7)$$

According to the Wiedemann - Franz law,[53] the electronic thermal conductivity (k_c) is associated with the carrier density (n), while the lattice thermal conductivity (k_l) can be independently modulated by introducing phonon scattering. Based on the theoretical analysis of these three key parameters, several strategies for enhancing thermoelectric performance are put forward: (1) Band engineering, including improving the symmetry of the crystal structure, multi-band degeneracy, and introducing electronic resonance states; (2) Lattice thermal conductivity can be reduced through phonon scattering, which involves introducing point defects (such as doping or alloying), constructing mesoscopic structures, and forming second-phase nanostructures; (3) Electrical conductivity and thermal conductivity can be decoupled via interface scattering in nanostructures.[13]

For a thermoelectric device, its maximum power conversion efficiency is given by the following Eq. (8):[57]

$$\eta_{max} = \frac{T_h - T_c}{T_h}\left(\frac{\sqrt{1+Z\overline{T}}-1}{\sqrt{1+Z\overline{T}}+\frac{T_c}{T_h}}\right) \quad (8)$$

According to the laws of thermodynamics, the conversion efficiency of a thermoelectric device is also limited by the Carnot cycle. Under the conditions of the hot side temperature T_h and the cold side temperature T_c, the maximum conversion efficiency is only determined by the ZT value.[59]

The thermoelectric properties of a material are determined by the dimensionless optimum ZT. To improve ZT, synergistic optimization of S, σ, and k is crucial, but the intrinsic coupling between them (*e.g.*, increasing carrier concentration raises σ but lowers S) requires advanced strategies. Nanostructure engineered phonon scattering plays a key role in reducing lattice thermal conductivity (k_l). For example, heterogeneous interfaces between MXene and CNTs are capable of scattering low and mid-frequency phonons, reducing k_l by 30 - 50%.[60] In addition, hierarchical porous structures (oriented freeze dried aerogels with hierarchical channels) further suppress phonon transport by increasing boundary scattering.[61] For "σ - S synergistic optimization", energy band engineering through chemical doping has shown promising results. For example, PEDOT:PSS doped with DBSA improved σ by a factor of two while maintaining S at 85% of the original value, which was achieved by balancing carrier concentration and energy filtering.[48]

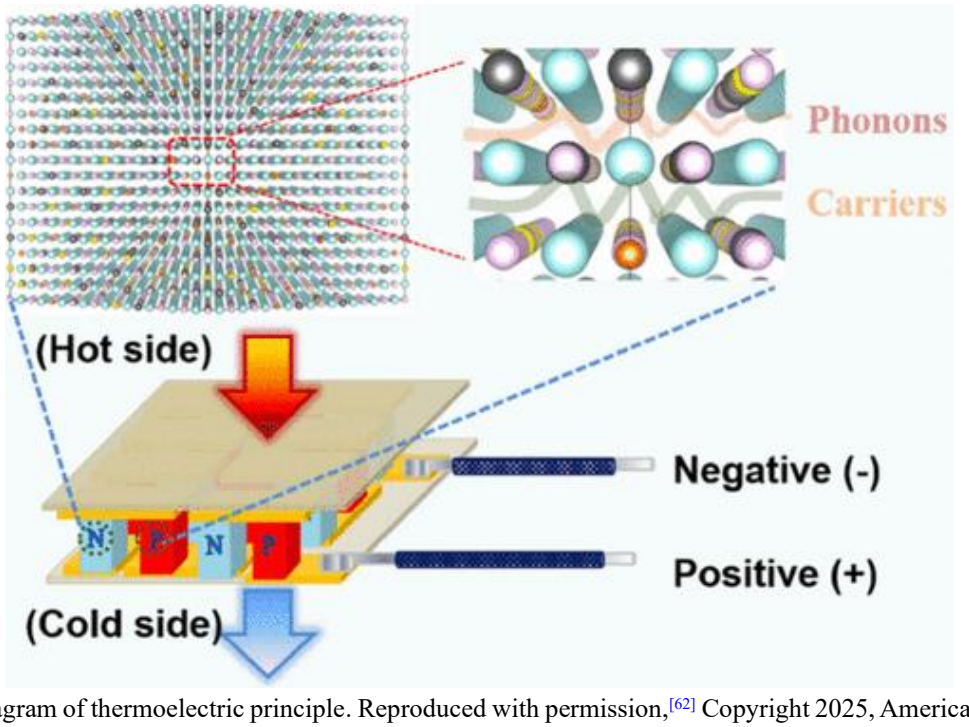

Fig. 1: Schematic diagram of thermoelectric principle. Reproduced with permission,[62] Copyright 2025, American Chemical Society.

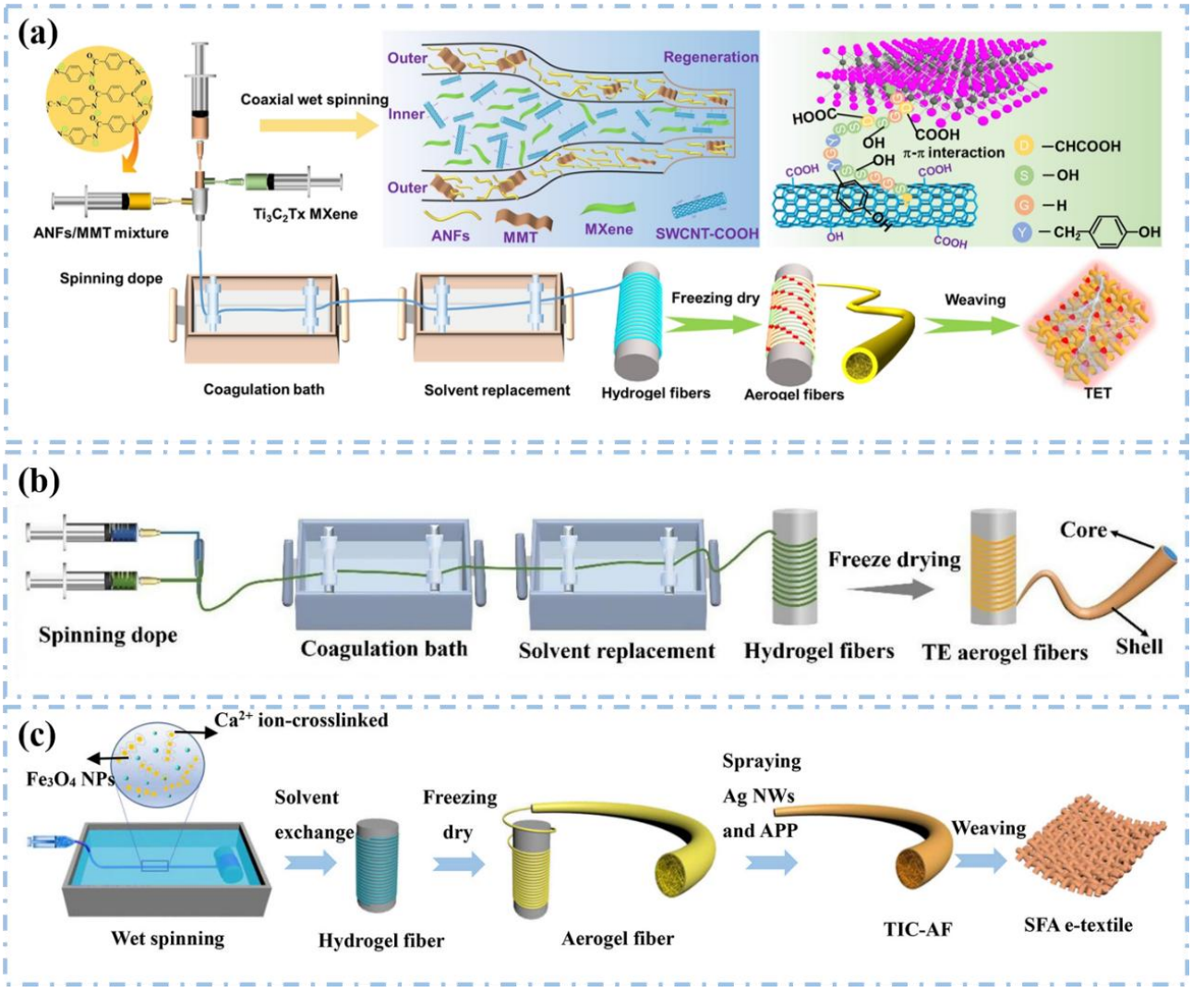

Fig. 2: **a** Schematic diagram of the preparation of p-n segment thermoelectric aerogel fibers by the alternate coaxial wet spinning strategy. Reproduced with permission,[60] Copyright 2023, The Author(s). **b** Schematic diagram of the preparation of core-shell structured SS/OSA@MXene thermoelectric fibers by the coaxial wet spinning method. Reproduced with permission,[69] Copyright 2024, Donghua University, Shanghai, China. **c** Schematic diagram of the preparation of MXene/Ag NWs/ANFs (MAA) aerogel fibers by the wet spinning technology. Reproduced with permission,[70] Copyright 2023, Elsevier Ltd.

3. Preparation methods and process innovation

Advanced preparation processes are the key to achieving high performance thermoelectric aerogels.[48,62] Different preparation processes can precisely control the microstructure and macroscopic shape of thermoelectric aerogels, thereby optimizing their thermoelectric and mechanical properties. Advanced preparation processes such as coaxial wet-spinning, freeze-drying technology, and 3D printing provide diverse options for the preparation of thermoelectric aerogels, meeting the requirements for material properties in different application scenarios.[63-65]

3.1 Wet-spinning technique

Wet spinning technology is a process that can be used to prepare fibers with special structures.[65] During operation, different spinning solutions are uniformly mixed and then extruded through a spinneret into a coagulation bath. The solution undergoes a coagulation reaction in the coagulation bath to form fibers with specific structures. This technology enables the compounding of various materials, effectively improving the comprehensive properties of the fibers.[66-68]

For example, He *et al*.[60] prepared p-n segment thermoelectric aerogel fibers by adopting an alternating coaxial wet-spinning strategy (Fig. 2a). First, the spinning dope with n-type Ti_3C_2Tx MXene and p-type MXene/SWCNT-COOH as the core materials, and the spinning dope with aramid nanofibers as the protective shell are prepared. By alternately injecting the spinning dope of the core material into the inner needle and the spinning dope of the protective shell material into the outer needle, it is solidified in the coagulation bath, and then the fiber is obtained after solvent replacement and freeze-drying. This spinning

technology can continuously produce fibers with an alternating p-n segment structure, endowing the fibers with both good flexibility and high-efficiency thermoelectric power both good flexibility and high-efficiency thermoelectric power generation performance. Moreover, the microstructure and performance of the fibers can be optimized by controlling the spinning process, such as forming a uniform concentric circle structure, ensuring the continuity and close fusion of the internal thermoelectric materials and the protective sleeve. Jiang *et al*.[69] prepared core-shell structured SS/OSA@MXene thermoelectric fibers via the coaxial wet-spinning method (Fig. 2b). Firstly, MXene nanosheets are prepared as the core layer material, and then the SS/OSA composite material with self-healing function is synthesized as the protective shell layer material. After the two materials are respectively made into spinning dope, they are injected into the inner needle and the outer needle through coaxial needles, solidified in a coagulation bath containing $CaCl_2$, and collected and freeze-dried to obtain the fibers. This technology can be used to prepare fibers with an adjustable core-shell structure, enabling the tight combination of the MXene in the core layer and the SS/OSA in the protective shell layer. It not only ensures the thermoelectric performance but also endows the fibers with characteristics such as self-healing and flame retardancy, improving the reliability and durability of the fibers. He *et al*.[70] prepared MXene/AgNWs/ANFs (MAA) aerogel fibers via wet-spinning technology (Fig. 2c). The prepared ANFs, MXene and AgNWs are respectively made into solutions, and the spinning solution is obtained by mixing them. After being injected into a pump-controlled syringe, the spinning solution is extruded through a needle into a coagulation bath (deionized water) to form hydrogel fibers, and then the MAA aerogel fibers are obtained after solvent replacement and freeze-drying. This technology is simple and feasible, and can effectively integrate a variety of functional materials (the thermoelectricity of MXene, the electrical conductivity of AgNWs, and the excellent comprehensive performance of ANFs) into the fibers, endowing the fibers with good flexibility, mechanical properties, as well as excellent temperature sensing and flame-retardant properties.

3.2 Freeze-drying technique

Freeze-drying technology optimizes the thermal conductivity of thermoelectric aerogels by regulating the porosity and pore size distribution. During the freeze-drying process, the solution containing the solute is first frozen into a solid state, and then the ice is directly sublimated in a vacuum environment to remove the solvent, leaving behind a porous solid structure. By controlling parameters such as freezing rate, freezing temperature, and sublimation conditions, the porosity and pore size distribution of thermoelectric aerogels can be precisely regulated.[71-74]

For example, He *et al*.[61] stated that freeze-drying technology is a crucial part of preparing aerogels with special properties. In the experiment, a mixed solution containing aramid nanofibers (ANFs), eicosane (C_{20}), MXene, MWCNTs, AgNWs and other components is first injected into a mold (Fig. 3a). Subsequently, the mold is placed on a copper plate in a liquid nitrogen atmosphere for directional freezing for 20 minutes, so that the solution is preliminarily formed. Then, the frozen sample is immersed in a mixed solution of ethanol and acetic acid for 48 h, followed by solvent exchange. Finally, the ACMCA aerogel is obtained after freeze-drying for 16 h. This directional freeze-drying strategy enables the aerogel to form a highly ordered layered porous structure similar to human muscle tissue. In terms of performance, the tensile strength of the aerogel reaches 2.52 MPa and the compressive strength is 0.21 MPa, demonstrating good mechanical properties. This allows it to withstand a certain amount of external force without being easily damaged when used as a material for fireproof suits. In terms of thermoelectric performance, its Seebeck coefficient at room temperature is as high as 46.78 $\mu V \cdot K^{-1}$ and the thermal conductivity is as low as 0.048 $W \cdot m^{-1} \cdot K^{-1}$, showing efficient thermoelectric conversion ability. When applied to fireproof suits, the aerogel can achieve wide temperature range sensing from 50 °C to 400 °C, and it performs excellently in high-temperature early warning with a response time of about 1.43 s, providing a strong guarantee for the safety of firefighters. Ren *et al*.[75] utilized bidirectional freezing and freeze-drying technologies to prepare biomimetic layered silica nanofiber/MXene aerogel (LSMA) in this study (Fig. 3b). Specifically, a homogeneous aqueous dispersion of MXene nanosheets, SNFs (silica nanofibers) and PVA (polyvinyl alcohol) is bidirectionally frozen. Under the combined action of a horizontal temperature gradient (ΔTH) and a vertical temperature gradient (ΔTV), the building blocks are pushed into the spaces between adjacent ice crystals and assembled into parallel thin sheets. Subsequently, the ice crystals are sublimated through freeze-drying, thus obtaining the LSMA aerogel with a microscopic structure resembling that of avian bones. This aerogel has an extremely low density, only 8.5 mg/cm³, and can stand independently on a foxtail grass, demonstrating its ultralight property. In terms of mechanical properties, it exhibits excellent anti-fatigue performance. After 10,000 compression cycles, its height retention rate can reach 99.1%, ranking among the top in the reported MXene-based aerogels. In the application of pressure-temperature dual-mode sensing, the LSMA sensor performs remarkably well, with a temperature resolution of up to 0.07 K and a pressure detection limit as low as 0.20 Pa, showing high sensitivity and high precision sensing performance. Li *et al*.[48] prepared the PEDOT:PSS/SWCNT composite aerogel via solution mixing, solvent replacement, and freeze-drying methods (Fig. 3c). Firstly, the SWCNT is dispersed by probe sonication in an ethanol solution for 60 minutes. Then, solvent replacement is realized through vacuum filtration to obtain an aqueous dispersion of SWCNT. Subsequently, NFC, an aqueous solution of PEDOT:PSS, and the cross-linking agent GOPS are added in sequence. After a series of ultrasonic and stirring treatments, the mixed solution

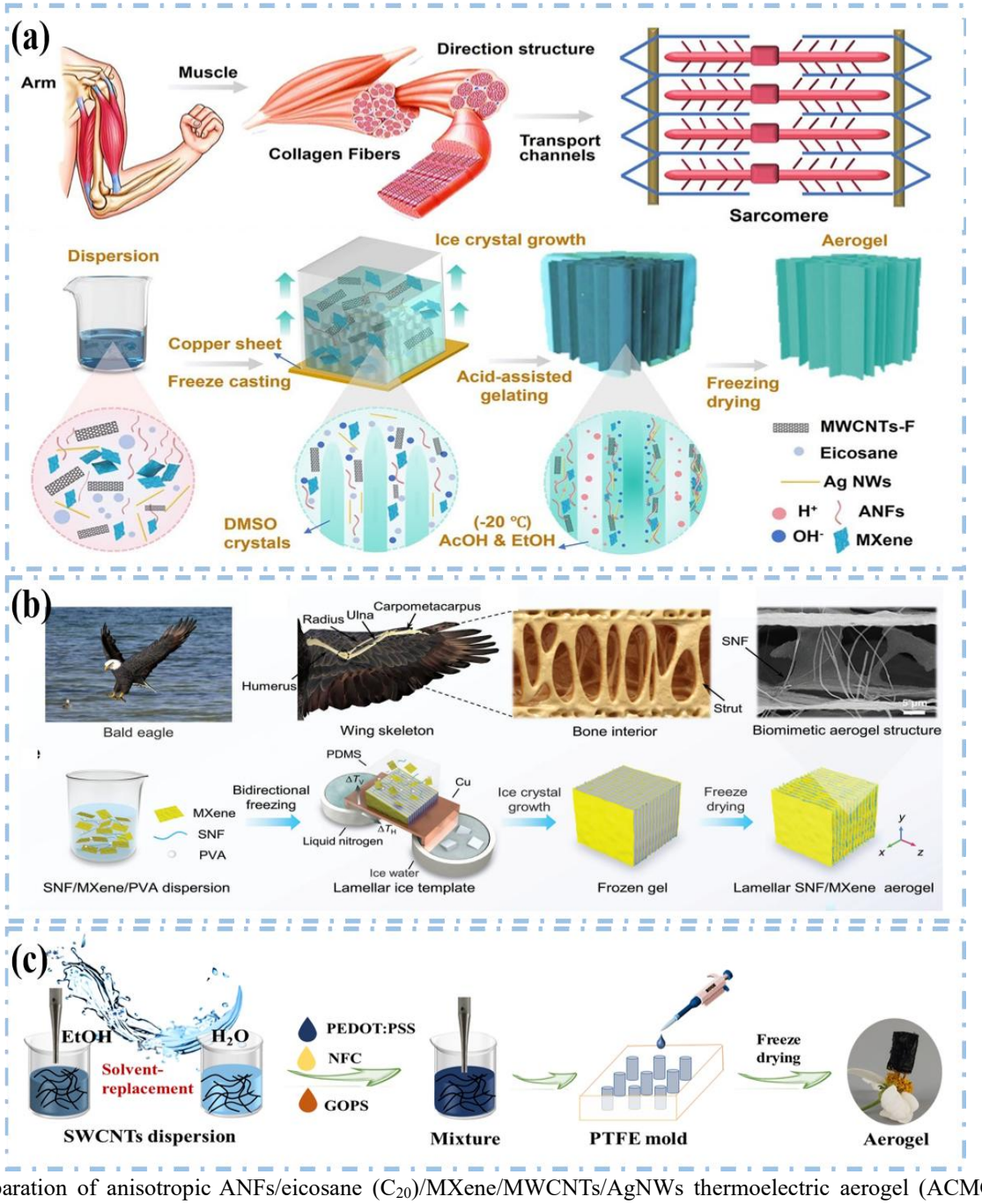

Fig. 3: **a** Preparation of anisotropic ANFs/eicosane (C_{20})/MXene/MWCNTs/AgNWs thermoelectric aerogel (ACMCA) via the directional freeze-drying strategy. Reproduced with permission,[61] Copyright 2025, The Author(s). **b** Preparation of biomimetic layered silica nanofiber/MXene aerogel (LSMA) by bidirectional freezing and freeze-drying technology. Reproduced with permission,[75] Copyright 2024, Wiley-VCH GmbH. **c** Preparation of PEDOT:PSS/SWCNT composite aerogel by the method of solution mixing, solvent replacement and freeze-drying. Reproduced with permission,[48] Copyright 2024, The Author(s).

is dropped into a PTFE mold. Finally, the aerogel is prepared by vacuum freeze-drying for 48 h. The aerogel prepared by this method presents a typical layered interconnected porous structure, with a porosity as high as 87%, a density as low as 0.01 g/cm³, and a thermal conductivity of 0.074 $W \cdot m^{-1} \cdot K^{-1}$. It also has super mechanical elasticity. The sensor constructed based on this aerogel can not only accurately detect pressure signals but also effectively sense temperature within a wide temperature range from 25 °C to 325 °C. In addition, a thermoelectric generator assembled from 25 such composite aerogels has excellent performance. It can generate a maximum output power of 400 μW under a temperature difference of 300 K, demonstrating good capabilities in high-temperature thermal energy harvesting and conversion.

3.3 3D printing technique

3D printing technology has brought new possibilities to the preparation of thermoelectric aerogels.[63] Through 3D printing, thermoelectric aerogels with complex structures can be customized to meet the special requirements for the shape and

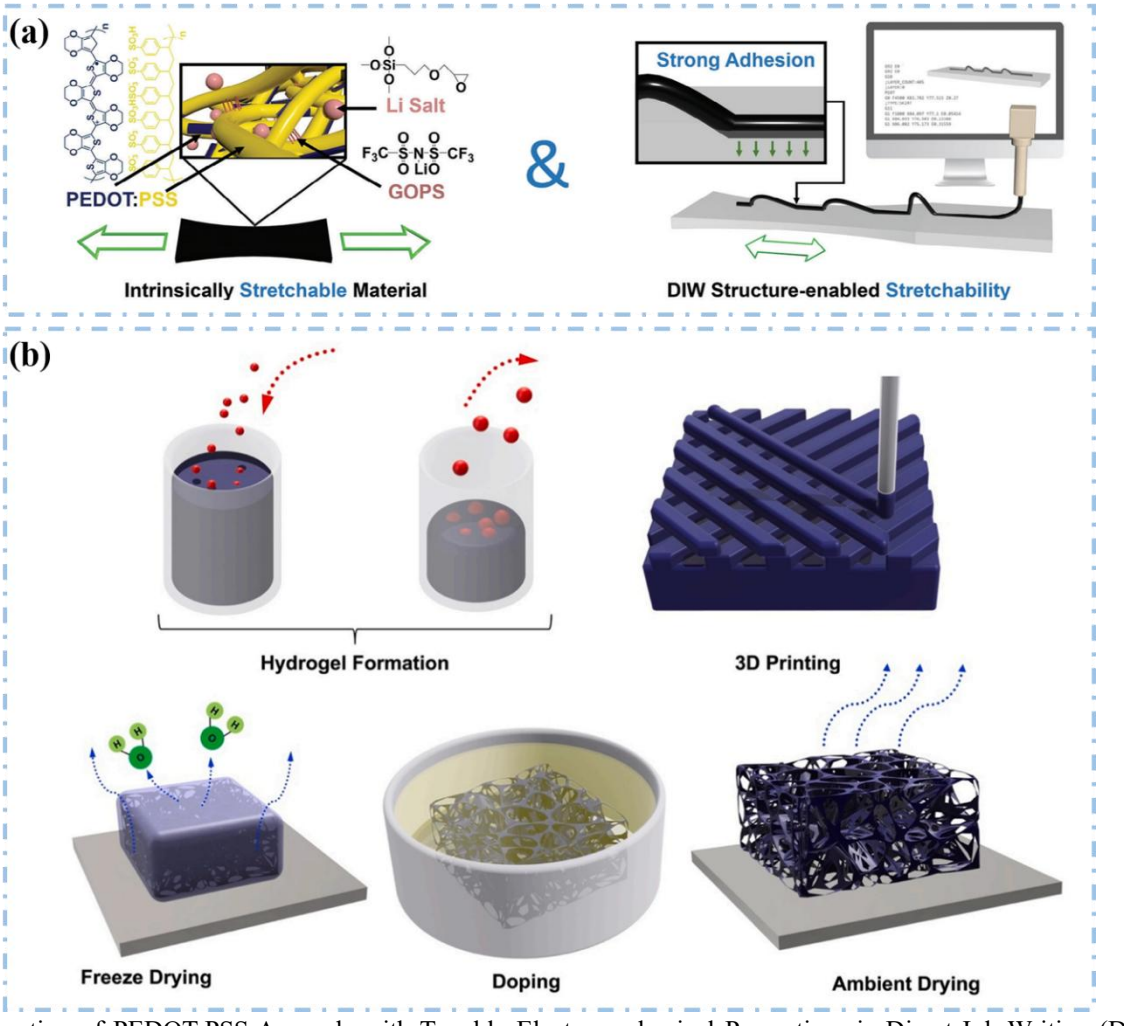

Fig. 4: **a** Preparation of PEDOT:PSS Aerogels with Tunable Electromechanical Properties via Direct Ink Writing (DIW) in 3D Printing Technology. Reproduced with permission,[79] Copyright 2025, The Author(s). **b** Combination of 3D Printing and Three-Stage Doping Process for Fabrication of PEDOT:PSS Aerogel Thermoelectric Generators. Reproduced with permission,[80] Copyright 2023, Elsevier Ltd.

function of materials in different application scenarios. During the preparation process, according to the designed 3D model, the printing ink containing the thermoelectric aerogel material is stacked layer by layer to finally form the desired structure.[76-78]

For example, Hasan Emre Baysal *et al*.[79]. employed the direct ink writing (DIW) method in 3D printing technology to prepare PEDOT:PSS aerogels with adjustable electromechanical properties in this study (Fig. 4a). First, a carefully formulated slurry containing Li salt and GOPS additives is printed into the desired structure on a stretchable substrate via DIW, and then freeze-drying is carried out to form a stable aerogel. Li *et al*.[80] combined 3D printing with a three level doping process to prepare a PEDOT:PSS aerogel thermoelectric generator in this study (Fig. 4b). Firstly, a hydrogel precursor with an appropriate concentration is prepared by mixing superabsorbent polymer (SAP) beads with a commercial PEDOT:PSS solution. Then, an aerogel with a controllable macroscopic and microscopic structure is obtained through 3D printing and freeze-drying. During the 3D printing process, by controlling the concentration of the hydrogel, precise regulation of key properties of the aerogel such as porosity, pore size distribution, thermal conductivity, electrical conductivity, and Seebeck coefficient can be achieved. For example, the aerogel printed at a concentration of 6 wt% has the highest porosity, the lowest thermal conductivity, and the highest *ZT* value. After that, the aerogel is subjected to three level doping. It is first soaked in a 0.3 M DBSA solution for 24 h, and then soaked in DMSO for 2 h. An aerogel with a high electrical conductivity of 27.15 S/cm, a low thermal conductivity of 75.38 $mW \cdot m^{-1} \cdot K^{-1}$, and a specific Seebeck coefficient of 19.34 μV/K is successfully prepared, and its *ZT* value reaches 3.99×10^{-3}, significantly improving the thermoelectric performance.

3.4 Comparative analysis of advantages and disadvantages of different preparation methods

In the preparation technology of thermoelectric gels, wet spinning, freeze-drying, and 3D printing are three core methods. The differences in their characteristics directly affect

the industrialization applications of materials. Drawing on existing research practices in thermoelectric gels, a comparative analysis can be carried out from three aspects: cost, process complexity, and large-scale production potential.

In terms of cost, wet spinning has a moderate cost. This method relies on continuous production equipment such as coaxial spinning nozzles and coagulation baths, with high material utilization rate, and can achieve stable output by adjusting spinning parameters. However, the solution preparation of multi component systems such as functional layers and protective layers in core sheath structures requires precise control of proportions, which may increase raw material mixing costs. Meanwhile, equipment maintenance such as nozzle cleaning and coagulation bath component renewal incurs ongoing expenses. Freeze-drying has relatively high costs. Its core processes include low-temperature freezing such as bidirectional temperature gradient control and vacuum freeze-drying, which consume substantial energy to maintain low-temperature environments such as liquid nitrogen. Additionally, the freeze-drying process takes a long time, resulting in significantly high energy consumption costs per unit product. Coupled with low equipment utilization due to batch processing mode, the comprehensive costs are further pushed up. 3D printing has the highest cost. This technology relies on high precision printing equipment such as omnidirectional nozzle systems and customized inks (which need to meet specific rheological properties), with high equipment procurement and maintenance costs. Moreover, the slow printing speed and low single batch output, along with time costs per unit product and material losses such as nozzle residues, further exacerbate cost pressures.

In terms of process complexity, wet spinning has moderate complexity. Its core lies in realizing shaping through phase separation of spinning solution in coagulation baths, requiring precise control of parameters such as spinning solution concentration, coagulation bath components, and extrusion rate. For multi-phase composite systems such as combinations of conductive and elastic layers, it is essential to prevent component delamination or agglomeration, and the difficulty of process control increases as structural complexity rises. Freeze-drying has higher complexity. The key is to induce specific porous structures such as lamellar or columnar pores through temperature gradients, requiring accurate regulation of freezing rate and temperature gradient direction to prevent disordered growth of ice crystals from damaging structural integrity. In the freeze-drying stage, ice crystals need to be sublimated slowly to prevent structural collapse such as interlayer cracking or pore shrinkage caused by stress concentration, which demands high operation accuracy. 3D printing has the highest complexity. Its core is to achieve stable extrusion and precise shaping of inks, requiring simultaneous optimization of ink rheological properties such as shear thinning characteristics, printing paths (to ensure interlayer bonding of complex structures), and post-treatments such as annealing to enhance performance. For high aspect ratio structures, nozzle clogging or structural distortion is prone to occur. Printing on flexible substrates also needs to solve interfacial adhesion issues, and the overall process is extremely sensitive to ambient temperature and humidity.

In terms of large-scale production potential, wet spinning has the strongest potential. This method is naturally suitable for continuous production, can increase output through multi nozzle parallel operation and automated winding, stably prepare fibrous or film products, and its product form is easy to integrate into end products such as textiles and flexible devices, showing outstanding mass production adaptability in fields like wearable devices and smart textiles. Freeze-drying has limited potential. It adopts batch processing mode, with single batch production volume limited by mold size. Moreover, the long-time consuming freezing and freeze-drying processes make continuous production difficult. In addition, large-area samples are prone to structural differences due to uneven temperature gradients, affecting product consistency, so it is more suitable for small batch preparation of high porosity and lightweight aerogels. 3D printing has weak potential. This technology relies on the "layer-by-layer stacking" forming method, with printing speed limited by nozzle movement speed and interlayer drying time, resulting in low single-batch output. Meanwhile, the printing precision of complex structures is susceptible to environmental factors, leading to poor batch stability, so it is more suitable for small batch customized products such as special shaped sensors and complex interconnection structures and difficult to meet the needs of large-scale industrial production.

In summary, wet spinning has significant advantages in mass production capacity and is suitable for large-scale scenarios with stable demand; freeze-drying excels in preparing high performance porous structures, but its high cost limits mass production; 3D printing has unique strengths in structural customization, making it better suited for high end small batch applications. The selection of the three methods should be comprehensively considered in combination with the cost budget, performance requirements, and mass production scale of specific application scenarios.

4. Performance optimization

Excellent structural properties are the key to achieving high performance thermoelectric aerogels. The high elasticity, flame retardancy, and mechanical strength of aerogels provide diverse options for the preparation of thermoelectric devices, meeting the requirements for material properties in different application scenarios.[81-84]

4.1 Mechanical properties

The excellent mechanical properties of aerogels enable them to have a wider range of applications. Yu *et al*.[61] revealed the structural and performance characteristics of ACMCA aerogels from multiple perspectives. Fig. 5a is a high magnification SEM image of the honeycomb structure on the surface of the ACMCA aerogel. From Fig. 5a, it can be clearly

seen that the cell walls of the aerogel are composed of interwoven ANFs, with a thickness of only a few micrometers. This microscopic structure is closely related to the macroscopic properties. The interwoven ANFs form a stable skeletal structure, which is the basis for the good mechanical properties of the aerogel. When actually applied to fire suits, this structure can effectively withstand external forces and ensure the safety of firefighters during rescue operations. At the same time, its unique porous structure helps to reduce the thermal conductivity, enhance the thermal insulation performance, and reduce the harm of external high-temperatures to firefighters. Fig. 5a$_1$ shows an optical photograph of the ACMCA aerogel placed on a flower. The aerogel has a regular size (with a side length of 3 cm and a thickness of 10 mm) and can be stably placed on the flower without damaging the flower structure. This intuitively reflects the ultralight characteristics of the aerogel, with a density of only 0.038 g/cm³. In the application of fire suits, this lightweight characteristic is crucial, as it can reduce the burden on firefighters, improve rescue efficiency, and enable firefighters to perform tasks more flexibly. Fig. 5a$_2$ presents optical images of the ACMCA aerogel in a bent state at 45° and 180°. The aerogel does not break even under such a large angle bending, fully demonstrating its excellent flexibility. This flexibility allows the ACMCA aerogel to adapt to various complex movements of firefighters in fire suits, and it will not be damaged due to frequent bending and stretching, ensuring the stability and reliability of the fire suit in different usage scenarios. It shows the scene where the ACMCA aerogel lifts a weight 400 times its own weight. This indicates that the aerogel has excellent strength and can withstand relatively large external forces.

In the actual use of fire suits, the aerogel with high strength can better protect firefighters, prevent damage caused by external forces such as collisions and pulls during the rescue process, and effectively improve the protective performance of the fire suit. Yu *et al*.[75] fabricated a super-fatigue-resistant MXene aerogel inspired by the structure of bird bones. Fig. 5b combined with the SEM image, shows the fatigue resistance mechanism of LSMA. The rigid MXene nanosheets are assembled into a highly ordered layered framework through bidirectional freezing, providing the basic structural support for the aerogel. The elastic SNFs are uniformly interspersed between the layers, acting like the supporting structure in bird bones, buffering the stress. Meanwhile, the adhesive effect of PVA and the entanglement and adhesion among the SNFs enable the MXene framework and SNFs to form a firm whole, allowing the stress to be uniformly transmitted and dispersed throughout the structure. In addition, the SNFs are embedded in the laminates and bridges, forming a structure similar to reinforced concrete, further enhancing the stability of the overall framework. This multi scale synergistic enhancement mechanism is the fundamental reason for the excellent fatigue resistance of LSMA.

Fig. 5c shows the compression stress strain curve of LSMA under 10,000 cycles at a strain of 50%. As can be seen from the curve, LSMA exhibits extremely excellent fatigue resistance. After 10,000 cycles, its plastic deformation is extremely low, only 0.9%. This characteristic benefits from its unique bionic structure. The elastic SNFs are uniformly distributed in the aerogel, similar to the supporting structure in bird bones, effectively enhancing the fatigue resistance of the aerogel. Compared with the unreinforced MXene aerogel, its fatigue resistance has been significantly improved, providing a solid foundation for LSMA to be used as a sensor material for long-term use. In wearable devices, if it is used to monitor human movement, it can withstand long-term deformation without failure, ensuring stable and reliable monitoring. Fig. 5c$_1$ presents the compression stress-strain situation of LSMA under different strains. It can be found that LSMA can still return to its initial height under a strain of up to 80%, reflecting its excellent compression resilience. Even if it is deformed under a large external force, it can quickly return to its original shape after the external force is removed. This characteristic enables LSMA to maintain the integrity of its structure when subjected to various pressures, ensuring that it will not be damaged due to frequent pressure changes in applications such as pressure-temperature dual-mode sensing, and extending its service life. Fig. 5c$_2$ shows the changes in the maximum stress, energy loss coefficient, and plastic deformation of LSMA under a strain of 50% with the number of compression cycles. As the number of cycles increases, the maximum stress remains above 79% of the initial value even after 10,000 cycles, and gradually tends to be stable; the energy loss coefficient and plastic deformation also gradually stabilize. This indicates that LSMA has good structural stability and reliable mechanical properties during long-term compression. When actually applied to sensors, it can ensure that during long-term use, the sensing performance for pressure and temperature will not be significantly affected by structural changes, ensuring the accuracy and stability of the sensors. He *et al*.[60] prepared p-n segmented coaxial aerogel fibers via wet-spinning. Fig. 5d shows the microstructure of the p-n segmented core-shell thermoelectric device fiber from different angles. The cross-sectional SEM image clearly demonstrates that the p-n segmented core-shell thermoelectric device fiber has a regular concentric circle structure. This structure indicates that the internal thermoelectric material and the continuous protective sheath have been successfully formed. The regular concentric circle structure is crucial for the performance of the fiber. The internal thermoelectric material is the core for achieving the self-powered fire alarm function, while the continuous protective sheath can effectively protect the internal thermoelectric material, enabling it to work stably in complex environments. In the actual application scenarios of fire suits, this structure can resist adverse factors such as external friction and high-temperatures, ensuring that the thermoelectric performance of the fiber is not affected and thus guaranteeing the reliability of the fire alarm function. From the middle SEM image, it can be

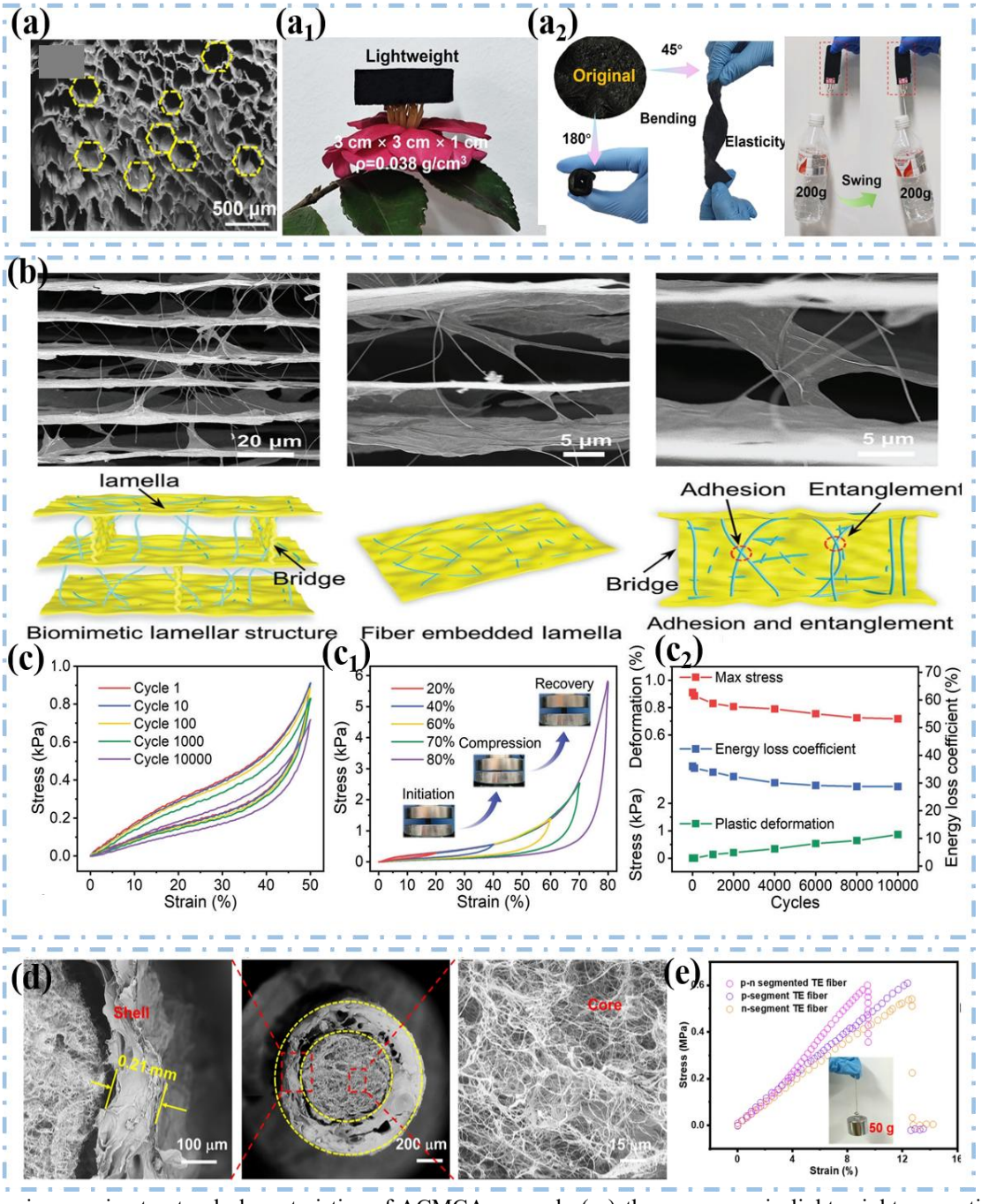

Fig. 5: **a** The microscopic structural characteristics of ACMCA aerogels (**a**$_1$) the macroscopic lightweight properties of CMCA aerogels (**a**$_2$) the flexibility and high strength of CMCA aerogels. Reproduced with permission,[61] Copyright 2025, The Author(s). **b** Schematic diagram of the fatigue resistance mechanism. **c** Compression stress-strain curve under 10,000 cycles with a strain of 50% (**c**$_1$) Compression stress-strain curves under different strains (**c**$_2$) Changes in relevant parameters with compression cycles under a strain of 50%. Reproduced with permission,[75] Copyright 2024, Wiley-VCH GmbH. **d** SEM image of p-n segmented coaxial aerogel fiber. **e** Tensile stress-strain curves of different thermoelectric device fibers. Reproduced with permission,[60] Copyright 2023, The Author(s).

seen that the outer diameter of the p-n segmented core-shell thermoelectric device fiber is 853.12±18.37 μm, and the wall thickness is 211±21.39 μm. Moreover, the core and the shell are continuously and closely integrated without obvious gaps and holes. The appropriate outer diameter and wall thickness ensure the mechanical strength of the fiber, making it less likely to be damaged during actual use. The closely integrated core-shell structure is beneficial for charge transfer, reducing energy loss and having a positive impact on improving the thermoelectric performance of the fiber. In fire suits, the stable structure can ensure that the fiber will not be damaged by external forces such as friction and stretching during the activities of firefighters, maintaining its normal working state. The right image shows that in the p-type MXene/SWCNT-

COOH core material, the SWCNT-COOH has a "spider web" morphology. This morphology reflects the good self-assembly compatibility between SWCNT-COOH and MXene. The good compatibility enables the two materials to work synergistically, enhancing the conductivity and other properties of the core material. During the thermoelectric conversion process, it is conducive to the transfer and movement of charges, thereby improving the overall thermoelectric performance of the fiber and providing strong support for achieving efficient self-powered fire alarms.

Fig. 5e shows the typical tensile stress-strain curves of the p-segment, n-segment, and alternating p-n segment thermoelectric device fibers. The p-segment thermoelectric device fiber has a maximum elongation of 12.4% under a tensile stress of 0.54 MPa; the n-segment thermoelectric device fiber has a maximum elongation of 12.7% under a tensile stress of 0.6 MPa; the p-n segment thermoelectric device fiber has a tensile strength of 0.56 MPa and an elongation at break of 9.4%. These data indicate that different types of fibers have differences in mechanical properties. The p-n segment thermoelectric device fiber has a certain tensile strength and elongation, which can meet the basic mechanical requirements in the application of fire suits, ensuring that the fiber will not break easily during the wearing process by firefighters and having good practicality.

4.2 Thermoelectric properties

Thermal electrical aerogels, with the synergy of unique porous structures and functional components, demonstrate excellent performance in the fields of thermoelectric conversion and temperature sensing. Their core advantages are mainly reflected in high conversion efficiency, wide temperature range response, high sensitivity, structural stability and other aspects. Yu *et al*.[61] reported that ACMCA aerogels prepared via a directional freeze-drying strategy exhibit a unique microstructure, enabling muscle-inspired anisotropic aramid nanofiber aerogels to achieve efficient thermoelectric conversion and precise temperature monitoring in firefighting suits. From the SEM images in Figs. 6a$_1$ and a$_2$, it can be clearly seen that the MXene nanosheets are orderly arranged along the directional freezing direction, forming a continuous conductive network, which greatly promotes the transport of charge carriers. This structural advantage endows the ACMCA aerogels with a low thermal conductivity (0.048 W m^{-1} K^{-1}), effectively reducing the heat loss, and thus significantly improving the thermoelectric conversion efficiency. Fig. 6a$_3$ shows the voltage output of the ACMCA aerogels at different temperatures. With the change of temperature, the voltage output shows a good linear relationship, further demonstrating its efficient thermoelectric conversion ability. This figure provides strong support for expounding the advantages of the thermoelectric conversion efficiency of the ACMCA aerogels.

Yu *et al*.[48] demonstrated that PEDOT:PSS/SWCNT composite aerogels prepared for high-temperature thermal energy utilization via elastic thermoelectric aerogels exhibit excellent thermoelectric properties under specific conditions. Fig. 6b shows the variation of the power factor of the composite aerogels under different compressive strains. When the strain is 80%, the power factor reaches 0.58 μW m^{-1} K^{-2}, reflecting the influence of strain on the thermoelectric properties, and also indirectly indicating the potential of the aerogels to achieve efficient thermoelectric conversion under different working conditions. Yu *et al*.[85] reported that the CNT/MXene/cellulose nanofiber aerogel (CMC) sensor, designed as a high-performance bimodal temperature-pressure contact sensor with enhanced multifunctionality based on layered CNT-MXene-cellulose nanofiber aerogels, exhibits excellent performance in temperature detection. Fig. 6c$_1$ shows that the Seebeck coefficient of this sensor is 33.5 μV K^{-1}. This relatively high Seebeck coefficient indicates that the sensor is extremely sensitive to temperature changes. Fig. 6c$_2$ further shows the voltage response of the CMC sensor to small temperature differences, with the minimum detectable temperature change as low as 0.03 K, fully demonstrating its advantages of high sensitivity in temperature sensing. These two figures provide key evidence for demonstrating the temperature sensing sensitivity of the thermal electrical aerogels.

Ren *et al*.[75] reported that the silica nanofiber/MXene aerogel (LSMA) sensor, inspired by bird bones to create a super anti-fatigue MXene aerogel with human-like tactile perception and machine learning-assisted multi-level information encryption capabilities, also demonstrates advantages in temperature sensing. Fig. 6d$_1$ shows the relationship between the thermoelectric voltage of the sensor and the temperature difference, and the Seebeck coefficient (S_T = -8.96 μV·K^{-1}) reflects its sensitivity to temperature changes. Fig. 6d$_2$ shows the response of the LSMA sensor to slight temperature stimuli, and it can detect a temperature difference as low as 0.07 K, further proving the advantages of thermal electrical aerogels in terms of temperature sensing sensitivity. Ren *et al*.[69] reported that SS/OSA@MXene self-healing core-sheath thermoelectric fibers prepared via a coaxial wet-spinning strategy for fire safety in firefighting suits maintain stable output voltage after multiple heating-cooling cycles. Fig. 6e shows that during 60 alternating heating and cooling cycles, the output voltage of the sensor remains at approximately 1.41 mV, which is close to the theoretical value, fully demonstrating its stability in temperature sensing. This figure intuitively reflects the stability advantage of thermal electrical aerogels in temperature cycling tests.

Ren *et al*.[61] reported that ACMCA aerogels demonstrate good stability in the study of muscle-inspired anisotropic aramid nanofiber aerogels, which exhibit efficient thermoelectric conversion and precise temperature monitoring in firefighting suits. Fig. 6f shows the variation of the output voltage of the ACMCA aerogels during 10 heating (at 250 °C) and cooling (at room temperature) cycles. After multiple cycles, its output voltage is stable with minimal fluctuations,

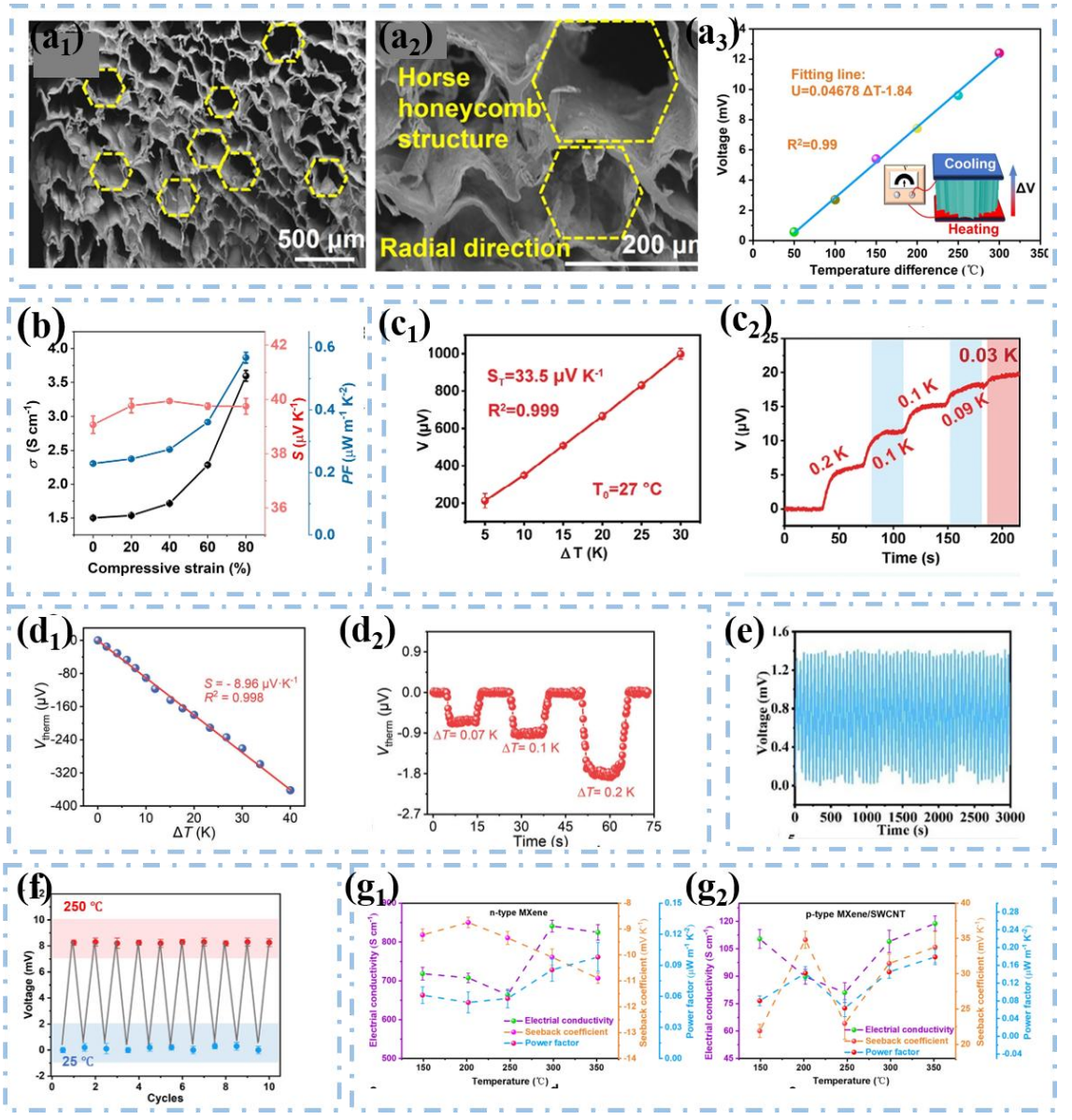

Fig. 6: **a**$_1$、**a**$_2$ SEM images of the honeycomb structure on the surface of the ACMCA aerogel at different magnifications. **a**$_3$ linear fitting curve of the output voltage of the ACMCA aerogel and the temperature difference. Reproduced with permission,[61] Copyright 2025, The Author(s).**b** the variation of the thermoelectric properties of the PEDOT:PSS/SWCNT composite aerogel with the compressive strain. Reproduced with permission,[48] Copyright 2024, The Author(s). **c**$_1$ the linear response characteristic diagram of the temperature gradient and output voltage of the sensor based on the CNT/MXene/cellulose nanofiber aerogel. **c**$_2$ The diagram of the voltage response characteristics of the CMC sensor to small temperature changes. Reproduced with permission,[85] Copyright 2024, Wiley-VCH GmbH.**d**$_1$ characteristic diagram of the temperature difference - thermoelectric voltage related to the Seebeck coefficient of the LSMA sensor based on MXene aerogel. **d**$_2$ diagram of the thermoelectric voltage response of the LSMA sensor to slight temperature stimuli. Reproduced with permission,[75] Copyright 2024, Wiley-VCH GmbH. **e** The diagram of the temperature sensing performance and stability test of the SS/OSA@MXene coaxial TE aerogel fibers. Reproduced with permission,[69] Copyright 2024, Donghua University, Shanghai, China. **f** The test diagram of the output voltage stability of ACMCA aerogel during 10 heating-cooling cycles between 250 °C and room temperature. Reproduced with permission,[61] Copyright 2025, The Author(s). **g**$_1$ The temperature-related thermoelectric characteristics of n-type MXene. **g**$_2$ The temperature-related thermoelectric characteristics of p-type MXene/SWCNT-COOH. Reproduced with permission,[60] Copyright 2023, The Author(s).

which further illustrates the stability advantage of thermal electrical aerogels in different temperature environments. He *et al*.[60] focused on the thermoelectric properties of p-n segment core-shell structured thermoelectric fibers in the study of temperature-sensing self-powered fire alarm electronic textiles based on p-n segment coaxial aerogel fibers for active fire prevention in firefighting suits. The temperature-related thermoelectric characteristics of the n-

type MXene and p-type MXene/SWCNT-COOH materials are presented, providing crucial evidence for understanding the performance advantages of these thermoelectric fibers. Fig. 6g$_1$ shows the changes in the thermoelectric properties of the n-type MXene material within the temperature range of 150 – 350 °C. As can be seen from the figure, the Seebeck coefficient is negative, indicating that the internal charge carriers are mainly electrons. With the increase of temperature, the absolute value of the Seebeck coefficient first decreases and then gradually increases, while the conductivity shows an opposite trend, exhibiting typical metallic behavior. This variation trend reflects the influence of the changes in carrier concentration and mobility of the n-type MXene material at different temperatures on its thermoelectric properties.In the p-n segment thermoelectric fiber system described in the paper, as one of the core materials, the n-type MXene's stability and controllability of thermoelectric properties are of great significance for the thermoelectric conversion efficiency of the entire fiber. This characteristic enables the p-n segment thermoelectric fibers to generate stable voltage signals through the Seebeck effect in different temperature environments, providing a reliable basis for temperature sensing in applications such as fire alarms. Fig. 6g$_2$ presents the changes in the thermoelectric properties of the p-type MXene/SWCNT-COOH material with temperature. Different from the n-type MXene, the Seebeck coefficient of this material is positive within the range of 150 – 350 °C, confirming the p-type characteristics of the carriers in it. Its power factor shows a similar temperature-dependent trend to the Seebeck coefficient. The Seebeck coefficient first increases, then decreases, and slowly rises again with the change of temperature, while the conductivity first decreases, reaching a minimum value of 81.05 S cm^{-1} at 250 °C and then increases. In the p-n segment thermoelectric fibers, the p-type MXene/SWCNT-COOH material and the n-type MXene cooperate with each other. The different thermoelectric properties of the two enable a stable potential difference to be formed at the p-n junction when the temperature changes, thus achieving efficient thermoelectric conversion. This complementary thermoelectric characteristic is one of the key factors that allow the p-n segment thermoelectric fibers to effectively convert thermal energy into electrical energy and realize the self-powered fire alarm function.

5. Application fields and typical cases

Thermoelectric aerogels have demonstrated great application potential in self - powered wearable systems, bringing new opportunities for the development of smart wearable devices.[61,86] As a typical representative of self-powered wearable systems, the smart sensing glove integrates various excellent properties of thermoelectric aerogels, achieving functions such as wide-temperature-range detection and gesture recognition, and providing users with a more intelligent and convenient interactive experience.[87-90]

5. 1 Smart sensing gloves

The advancement of intelligent sensing technology has led to an increasing demand for multifunctional electronic devices.[91-93] Thermoelectric aerogels, with their unique thermoelectric properties, lightweight nature, and high elasticity, inject new vitality into the performance improvement and functional expansion of intelligent sensing gloves, revolutionizing the gloves performance in aspects such as temperature monitoring, motion recognition, and environmental interaction.[60] Tian *et al*.[85] demonstrated that the developed layered CNT/MXene/cellulose aerogel (CMC) sensor gloves exhibit excellent temperature resolution. As shown in Figs. 7a$_1$-a$_4$,when the wearer comes into contact with a cold water cup (15 °C) and a hot water cup (50 °C), the thermal voltage signal maps of the fingertip and palm regions of the gloves show significant differences: the cold water triggers a low-temperature response of approximately -0.8 mV, while the hot water generates a high-temperature signal of +1.2 mV, clearly reflecting the temperature distribution on the hand surface (with a resolution of 0.03 K). The stable temperature gradient supported by the low thermal conductivity (0.056 W·m^{-1}·K^{-1}) makes it suitable for daily temperature sensing monitoring of rheumatism patients. Li *et al*.[48] showed that the PEDOT:PSS/SWCNT aerogel gloves can detect temperatures over a wide range from 25 °C to 325 °C. Figs. 7b$_1$-b$_3$ show that when the finger touches a metal plate heated to 200 °C, the sensor outputs a voltage of 4.6 mV, and there is no signal attenuation when the compression strain reaches 60%. This compression resistance (the conductivity increases to 3.7 S·cm^{-1} under 80% strain) makes it an ideal choice for scenarios such as boiler inspection and metallurgical operations, and it can provide real-time early warnings of high-temperature contact risks (for example, triggering a buzzer alarm when the temperature is higher than 250 °C). Tian *et al*.[85] demonstrated that thermoelectric aerogel gloves, leveraging the synergy of piezoresistive and thermoelectric effects, can achieve precise recognition of complex hand gestures. The CMC sensor array (as shown in Figs. 7c$_1$-c$_3$) can successfully distinguish three typical postures by monitoring the pressure distribution when holding a pen. These postures include the correct grip posture (with concentrated pressure on the fingertips and a 58.8% decrease in resistance), the incorrect grip posture (with abnormal pressure on the palm and a resistance fluctuation of ± 20%), and the relaxed state (with no significant change in resistance). The combination of this high sensitivity (-45.2 %·kPa^{-1}) with machine learning enables the gloves to accurately capture actions such as "pointing", "pinching", and "grasping" during virtual reality interactions. Ren *et al*.[75] developed bionic bird bone MXene aerogel gloves. As shown in Figs. 7d$_1$-d$_4$, the 3×3 sensing array collaboratively inputs the password "1579" through a plastic rod (pressure input) and a finger (temperature input). The pressure signal (a 30% decrease in resistance corresponding to 1 kPa) and the thermoelectric signal (a

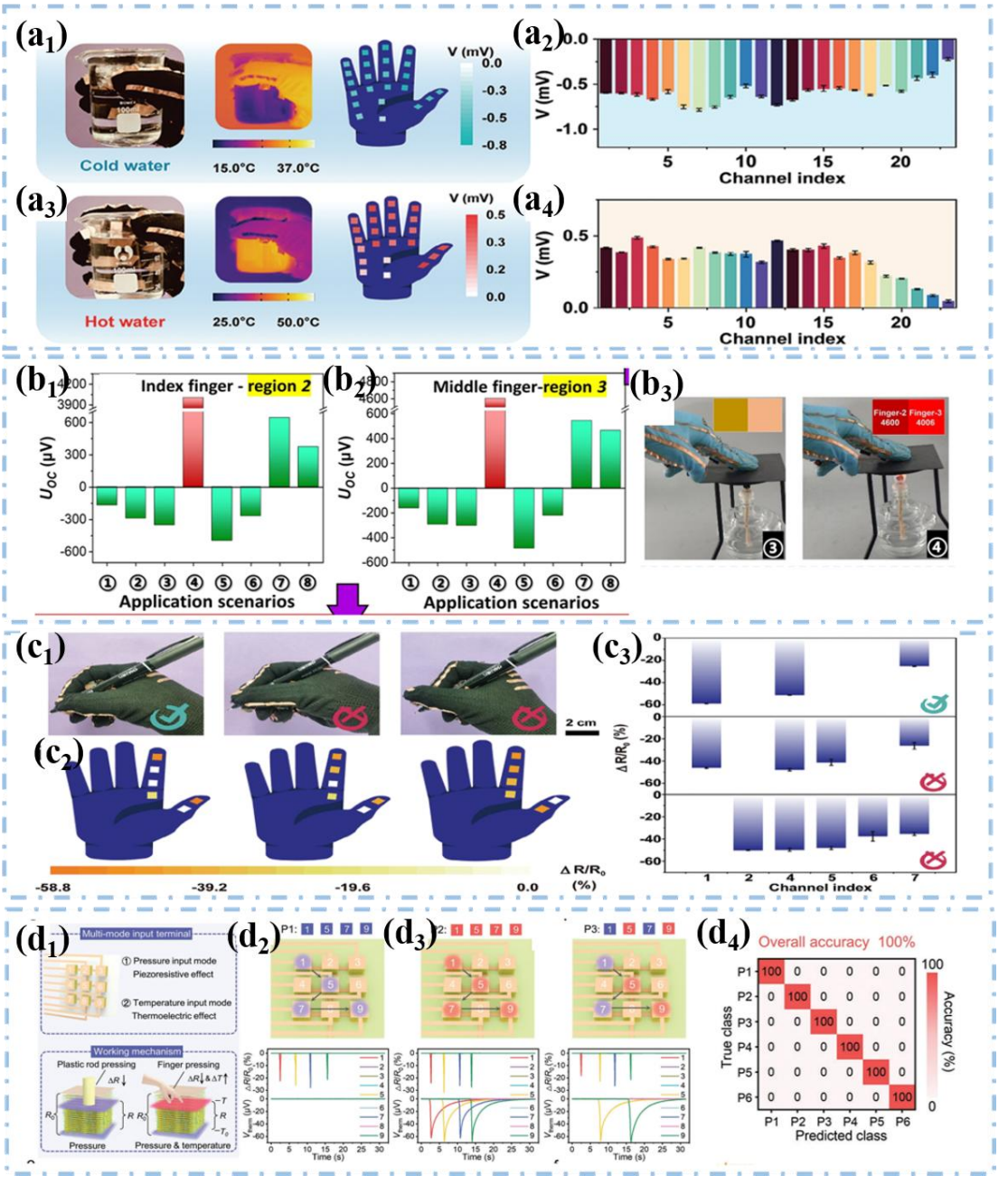

Fig. 7: **a1- a4** The thermal voltage map of the gloves when they contact cold and hot water cups. The signal change corresponding to the temperature difference from 15 °C to 50 °C. Reproduced with permission,[85] Copyright 2024, Wiley-VCH GmbH. **b1- b3** The voltage signal in the high-temperature touch experiment. Reproduced with permission,[48] Copyright 2024, The Author(s). **c1- c3** The resistance change and pressure distribution thermal map of three pen-holding postures. Reproduced with permission,[85] Copyright 2024, Wiley-VCH GmbH. **d1-d4** The dual-modal signals of the 3×3 array when inputting "1579" and the confusion matrix. Reproduced with permission,[75] Copyright 2024, Wiley-VCH GmbH.

voltage of 179 μV generated when ΔT = 20 K) are processed by the CNN algorithm. The confusion matrix reveals a 100% classification accuracy. This dual-factor input mode of "pressure coding + temperature verification" offers an interaction solution with a higher security level for the control of confidential devices.

5.2 Integration of firefighting suits

In addition to the intelligent sensing gloves, thermoelectric aerogels have also made important progress in the integration of firefighting suits, providing more reliable protection for the safety of fire fighters.[94-96] Thermoelectric aerogels, with their unique thermoelectric conversion ability and thermal protection performance, have become the core material for enhancing the intelligent safety protection of firefighting suits. Taking the muscle-bionic anisotropic aramid nanofiber aerogel (ACMCA) as an example, its deep integration with the multi-level wireless alarm system provides an innovative

solution for the safety of firefighters in extreme fire environments.[61]

Based on the efficient thermoelectric conversion and precise temperature-sensing capabilities of the fabricated ACMCA aerogel, it is integrated with the developed multi-level wireless high-temperature alarm system into firefighting suits. The developed hierarchical self-driven multi-level wireless alarm system, with dimensions of (3 cm×3 cm×1 cm), can be integrated into firefighting protective clothing together with ACMCA. The self-driven high-temperature alarm system based on ACMCA can achieve precise high-temperature monitoring of firefighting suits before they suffer thermal damage in a fire. In this temperature monitoring and early-warning system, preset thresholds are established for high and low temperatures, and three different-colored LED lights are used as indicators for the "safe", "high-temperature alert", and "warning" states of the firefighting suits.To verify the precise high-temperature early-warning function of the ACMCA aerogel, the temperature-sensing ACMCA aerogel is fixed on a temperature-controlled platform and connected to the wireless alarm system, and the early-warning is triggered by the thermoelectric generation of ACMCA. The alarm state threshold of the second-level early-warning system is set at 200 °C, and the danger alarm state threshold of the third-level early-warning system is set at 400 °C, corresponding to output voltage thresholds of 6.8 mV and 15.6 mV, respectively. To verify the accuracy of the hierarchical early-warning of the ACMCA aerogel, we heat the thermoelectric aerogel at different temperatures. When there is no temperature change, everything remains quiet. However, once the temperature is detected, the early-warning system is quickly activated and displays different levels of early-warnings (Fig. 8a). When the temperature of the aerogel is lower than 200 °C, a green light is triggered to indicate the "safe state" (first-level early-warning); when the temperature is between 200 - 400 °C, a yellow light is triggered to indicate the "high-temperature alert state" (second-level early-warning); when the temperature exceeds 400 °C, a red light is triggered (third-level early-warning).

The traditional thermal insulation layers of firefighting suits rely on passive thermal protection and lack the ability for real-time temperature monitoring. However, the ACMCA aerogel constructs an anisotropic structure through directional freeze-drying technology, achieving an integrated design of an intelligent thermal insulation layer and self-driven temperature sensing (Fig. 8b). Among them, the negative temperature coefficient phase-change material eicosane (C_{20}) works in concert with the MXene conductive network, endowing it with efficient thermal-barrier characteristics. With an ultra-low thermal conductivity of (0.048 $W \cdot m^{-1} \cdot K^{-1}$) and a significant temperature gradient effect, its surface equilibrium temperature is only 110.4 °C in a high-temperature environment of 300 °C, with a temperature difference of 189.6 °C, effectively blocking heat penetration. The MXene nanosheets arranged along the directional freezing direction form a continuous conductive channel, with a Seebeck coefficient as high as 46.78 $\mu V \cdot K^{-1}$, which can directly convert the temperature difference into an electrical signal, realizing self-driven thermoelectric conversion and avoiding the failure risk of traditional sensors relying on external power sources.

To simulate the durability performance of ACMCA during the actual wearing of firefighting suits, cyclic compression tests are carried out on the electrical conductivity of ACMCA. Fig. 8c shows the compression stress-strain curve of ACMCA under 500 compression cycles at a strain of 20%. The results show that due to its anisotropic structure, ACMCA exhibits stable compressive performance and super-strong fatigue resistance. Figs. 8d and 8e show the resistance change rate [$(R - R_0)/R_0$] and the thermoelectric output voltage change rate [$(V - V_0)/V_0$] during the cyclic compression process. After 500 compressions, the resistance change rate and voltage change rate of ACMCA only change slightly, showing excellent electrical-related stability. In addition, add a resistance change test with a 10% compression strain and 10 cycles, further demonstrating the excellent stability of the ACMCA aerogel.

In addition, Fig. 8f further depicts the multi-level early-warning data diagram and logical design of the high-temperature alarm system. The electronic design automation schematic diagram of the alarm system shows that this early-warning system mainly includes modules such as voltage acquisition and processing, display circuit, indicator lights of different levels, calibration button, communication module, voltage reference, power supply circuit, and STM32 micro-controller unit. The ACMCA aerogel generates a thermoelectric voltage signal at high-temperatures, which is collected by the micro-controller to reflect temperature changes. When the voltage signal exceeds the early-warning trigger threshold, the wireless transmitter sends an instruction to the terminal receiver. Correspondingly, the wireless signal activates the indicator lights, allowing firefighters to quickly understand the safety status of the protective clothing according to the color of the indicator lights. The above results show that the multi-level wireless alarm system based on ACMCA has a promising application prospect in real-time temperature monitoring and multi-level high-temperature early-warning capabilities.

Fig. 8g depicts the extended application of ACMCA or ACMCA-M aerogel in firefighting suits, which can achieve ultra-sensitive temperature and visual toxic gas monitoring in complex fire environments. In a high-temperature environment, the aerogel can monitor the temperature of the surface of the insulation layer in real-time based on the linear relationship between the temperature difference and voltage. When the output voltage exceeds the set threshold, the wireless alarm system sends an early warning signal to the terminal via Bluetooth transmission. The activated indicator lights in the firefighting suit or the danger signals received by the firefighting base station can remind firefighters to evacuate in time before their lives are endangered. Overall, the

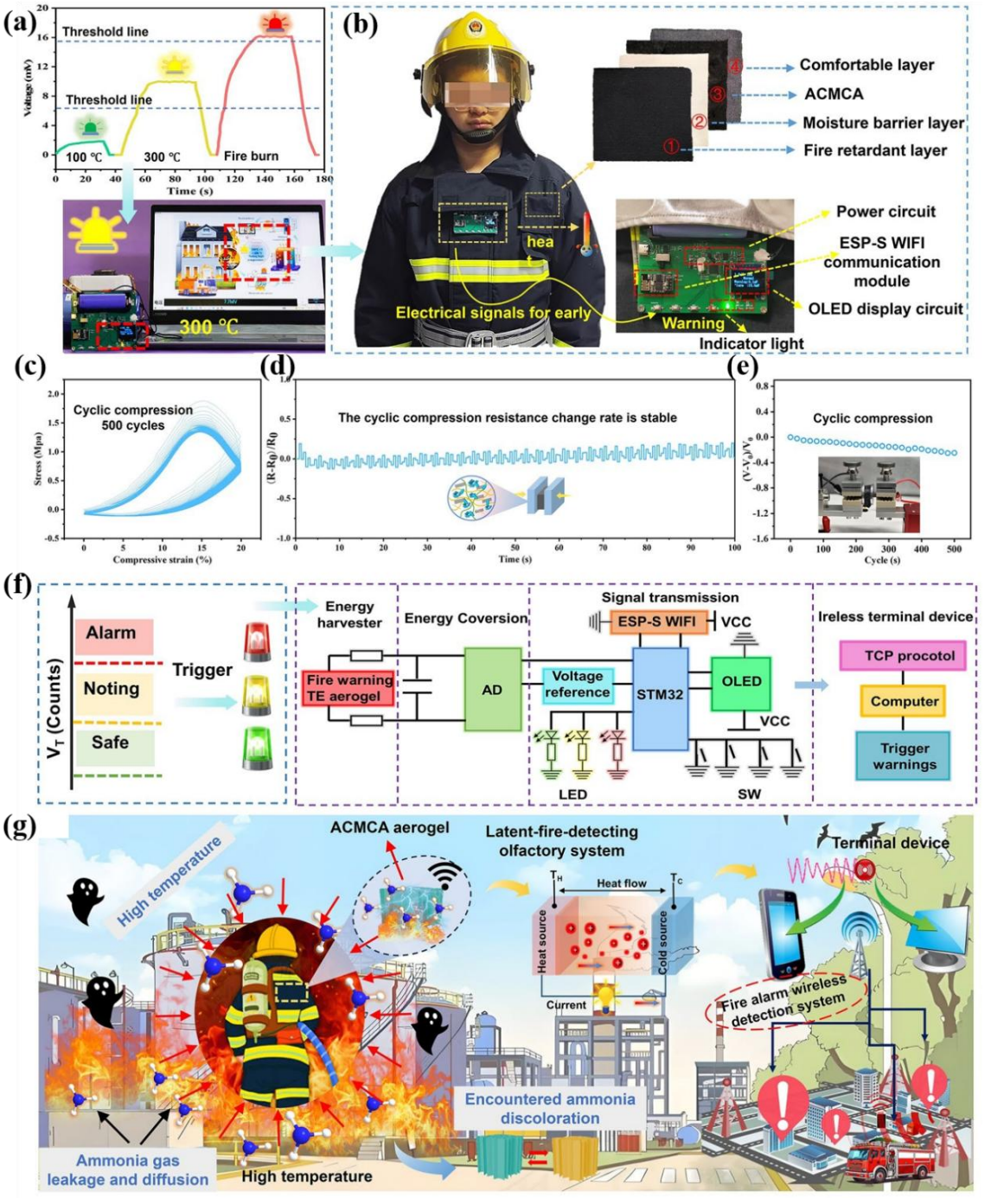

Fig. 8: **a** Multi-level high-temperature alarm test. **b** Schematic diagram of the layered structure of the firefighting suit. **c-e** Cycle compression performance curve. **f** Schematic diagram of the electronic design of the alarm system. **g** Schematic diagram of applications in complex fire scenes. Reproduced with permission,[61] Copyright 2025, The Author(s).

anisotropic thermoelectric aerogel inspired by human muscles can ensure the operational safety of firefighters in the face of complex fire environments that include high-temperatures and even flammable and explosive gases.

The integration of thermoelectric aerogels in firefighting suits has achieved a leap from passive protection to an active intelligent safety system. In the future, it is possible to further explore the integration with flexible energy storage devices and biological sign monitoring, and promote the upgrading of firefighting suits to full-scene intelligent protective equipment. Thermoelectric generators are based on the Seebeck effect and can directly convert heat energy into electrical energy. Their structure includes thermoelectric modules, heat exchangers, etc. They can recover waste heat in industry, utilize exhaust heat in vehicles, and supply power in special scenarios such as aerospace. Although their current conversion efficiency is limited and costs are high,[97-100] they have great development potential thanks to advantages like having no moving parts and being clean.[101-103] This also represents an expansion of the application fields of thermoelectric aerogels.

6. Summary and development prospect

Thermoelectric gels are a class of cutting-edge materials that fuse lightweight porous structures with thermoelectric conversion capabilities, and have made significant advances in the field of materials science and engineering. Their microstructures and macroscopic morphologies can be precisely tuned by advanced fabrication techniques (*e.g.*, coaxial wet spinning, freeze-drying, and 3D printing) to optimize the thermoelectric and mechanical properties for diverse applications.

In terms of functional applications, these gels demonstrate strong scene adaptability. In the field of fire safety, they enable a self-powered, multi-stage high-temperature warning system as the core insulation of firefighting suits. Through green/yellow/red indicator lights and wireless transmission, they dynamically monitor heat damage in real-time, buying critical evacuation time for firefighters. In wearable electronics, its pressure-temperature dual-mode sensing has given rise to self-powered smart gloves and flexible textiles that can differentiate complex hand movements (e.g., grasping, pointing) by voltage changes and track temperature differences of contacting objects (*e.g.*, ice water, warm water, hot water), which are promising for human computer interaction and medical health monitoring. In the industrial energy sector, flexible generators consisting of tandem aerogel units wrapped around high-temperature pipes for waste heat recovery synchronized with overheating alarms bring innovation in energy efficiency and safety of industrial processes.

However, in terms of performance, the dimensionless figure of merit (*ZT*) remains low (10^{-6} to 10^{-3}) due to the mutual constraints of conductivity, Seebeck coefficient and thermal conductivity. This is the result of a trade-off between the porous structure reducing thermal conductivity but disrupting electron transport. In contrast, bulk materials like Bi_2Te_3-based alloys have a ZT > 1. This disparity stems from three factors: (1) The porous structure of the aerogel leads to enhanced electron scattering (grain boundary scattering, pore interface scattering), resulting in a significant decrease in carrier mobility. Additionally, the low density and the possible increase in the proportion of amorphous materials further hinder the long-range transport of electrons, leading to a significant reduction in conductivity. In summary, the decrease in thermal conductivity is limited and cannot compensate for the decline in $S^2\sigma$; (2) The weak interfacial bonding in composites (*e.g.*, MXene-silica gel matrix) reduces carrier mobility; (3) The degradation of organic components under extreme conditions (*e.g.*, PEDOT:PSS collapses above 200 °C and MXene oxidizes at high humidity, with a conductivity drop of 30 - 50% in 100 h).

In addition to the *ZT* gap, thermoelectric gels face other key challenges. (1) Outstanding performance-mechanical conflict: Increasing electrical conductivity through densification, *e.g.*, reducing porosity, often comes at the expense of mechanical flexibility. (2) Scalable manufacturing bottlenecks: Existing processes make it difficult to produce large-area aerogels with uniform properties. (3) Multimodal signal crosstalk: In pressure-temperature dual-mode sensors, the piezoresistive effect of aerogel causes strain-induced resistance changes that mask the thermoelectric voltage signal, leading to temperature measurement errors during mechanical deformation. (4) Performance stability in harsh environments: PEDOT:PSS aerogel will experience structural collapse above 200 °C.

In response to the current problems and challenges, mitigation strategies include: encapsulation with PDMS coatings or silk gum and sodium alginate oxide shell layer, which can reduce MXene oxidation and improve washing resistance, with minimal loss of conductivity after 120 h of washing; chemical cross-linking can be added with GOPS, so that the PEDOT:PSS aerogel retains 80% of its initial conductivity for 500 h at 150 °C; and the structural design can be made by adopting a layered strut structure that mimics the skeleton of birds to disperse the deformation stress and reduce the loss of conductivity. The structural design can be modeled after the skeleton of birds by adopting a laminated column structure to disperse deformation stress and reduce water penetration, thus extending the service life in humid environments.

In the future, research needs to focus on four areas: (1) Through interfacial engineering to enhance MXene adhesion to polymers through coupling agents, balancing conductivity and insulation with the goal of doubling the *ZT* value; (2) Biomimetic structural optimization to develop highly fatigue-resistant aerogels that retain 99% of their height after 10,000 compression cycles, drawing on the structure of bird bones and muscle fibers; (3) Scalable process innovation requires optimization of 3D printing parameters and coaxial wet-spinning bath concentration to achieve large-area homogeneous production; (4) Multifunctional integration can be achieved by combining heterogeneous layered structures with energy storage units to build self-sustaining systems for remote monitoring of extreme environments.

In summary, the lightweight, flexible, and self-powered properties of thermoelectric aerogels render them transformative in the fields of intelligent sensing and energy conversion. Addressing performance, fabrication, and durability issues through interdisciplinary innovation will drive its large-scale application in fire safety, wearables, and industrial energy, contributing to a green, low carbon, and self-driven smart society.

Acknowledgments

This work was supported by the Postdoctoral Fellowship Program (Grade B) of China Postdoctoral Science Foundation under Grant Number GZB20240675.

Conflict of Interest

There is no conflict of interest.

Supporting Information
Not applicable.

References
[1] T. Xu, Z. Zhang, L. Qu, Graphene-based fibers: recent advances in preparation and application, *Advanced Materials*, 2020, **32**, 1901979, doi: 10.1002/adma.201901979.
[2] Y. Jia, Q. Jiang, H. Sun, P. Liu, D. Hu, Y. Pei, W. Liu, X. Crispin, S. Fabiano, Y. Ma, Y. Cao, Wearable thermoelectric materials and devices for self-powered electronic systems, *Advanced Materials*, 2021, **33**, e2102990, doi: 10.1002/adma.202102990.
[3] N. Wen, Z. Fan, S. Yang, Y. Zhao, C. Li, T. Cong, H. Huang, J. Zhang, X. Guan, L. Pan, High-performance stretchable thermoelectric fibers for wearable electronics, *Chemical Engineering Journal*, 2021, **426**, 130816, doi: 10.1016/j.cej.2021.130816.
[4] S. Darabi, M. Hummel, S. Rantasalo, M. Rissanen, I. Ö. Månsson, H. Hilke, B. Hwang, M. Skrifvars, M. M. Hamedi, H. Sixta, A. Lund, C. Müller, Green conducting cellulose yarns for machine-sewn electronic textiles, *ACS Applied Materials & Interfaces*, 2020, **12**, 56403-56412, doi: 10.1021/acsami.0c15399.
[5] Y. Liu, W. Zhou, W. L. Teo, K. Wang, L. Zhang, Y. Zeng, Y. Zhao, Covalent-organic-framework-based composite materials, *Chem*, 2020, **6**, 3172-3202, doi: 10.1016/j.chempr.2020.08.021.
[6] T. Ding, Y. Zhou, X.-Q. Wang, C. Zhang, T. Li, Y. Cheng, W. Lu, J. He, G. W. Ho, All-soft and stretchable thermogalvanic gel fabric for antideformity body heat harvesting wearable, *Advanced Energy Materials*, 2021, **11**, 2102219, doi: 10.1002/aenm.202102219.
[7] Y. Lin, J. Liu, X. Wang, J. Xu, P. Liu, G. Nie, C. Liu, F. Jiang, An integral p-n connected all-graphene fiber boosting wearable thermoelectric energy harvesting, *Composites Communications*, 2019, **16**, 79-83, doi: 10.1016/j.coco.2019.09.002.
[8] T. Sun, B. Zhou, Q. Zheng, L. Wang, W. Jiang, G. J. Snyder, Stretchable fabric generates electric power from woven thermoelectric fibers, *Nature Communications*, 2020, **11**, 572, doi: 10.1038/s41467-020-14399-6.
[9] Y. Du, K. F. Cai, S. Z. Shen, R. Donelsonand, J. Y. Xu, H. X. Wang, T. Lin, Multifold enhancement of the output power of flexible thermoelectric generators made from cotton fabrics coated with conducting polymer, *RSC Advances*, 2017, **7**, 43737-43742, doi: 10.1039/C7RA08663F.
[10] L. Liang, G. Chen, C. Y. Guo, Enhanced thermoelectric performance by self-assembled layered morphology of polypyrrole nanowire/single-walled carbon nanotube composites, *Composites Science and Technology*, 2016, **129**, 130-136, doi: 10.1016/j.compscitech.2016.04.023.
[11] L. Zhang, X. L. Shi, Y. L. Yang, Z. G. Chen, Flexible thermoelectric materials and devices: from materials to applications, *Materials Today*, 2021, **46**, 62-108, doi: 10.1016/j.mattod.2021.02.016.
[12] L. Wang, J. Zhang, Y. Guo, X. Chen, X. Jin, Q. Yang, K. Zhang, S. Wang, Y. Qiu, Fabrication of core-shell structured poly(3, 4-ethylenedioxythiophene)/carbon nanotube hybrids with enhanced thermoelectric power factors, *Carbon*, 2019, **148**, 290-296, doi: 10.1016/j.carbon.2019.03.088.
[13] G. Tan, L. D. Zhao, M. G. Kanatzidis, Rationally designing high-performance bulk thermoelectric materials, *Chemical Reviews*, 2016, **116**, 12123-12149, doi: 10.1021/acs.chemrev.6b00255.
[14] C. Gao, Y. Liu, Y. Gao, Y. Zhou, X. Zhou, X. Yin, C. Pan, C. Yang, H. Wang, G. Chen, L. Wang, High-performance n-type thermoelectric composites of acridones with tethered tertiary amines and carbon nanotubes, *Journal of Materials Chemistry A*, 2018, **6**, 20161-20169, doi: 10.1039/C8TA08045C.
[15] L. Yang, Z. G. Chen, M. S. Dargusch, J. Zou, High performance thermoelectric materials: progress and their applications, *Advanced Energy Materials*, 2018, **8**, 1701797, doi: 10.1002/aenm.201701797.
[16] H. Xu, Y. Guo, B. Wu, C. Hou, Q. Zhang, Y. Li, H. Wang, Highly integrable thermoelectric fiber, *ACS Applied Materials & Interfaces*, 2020, **12**, 33297-33304, doi: 10.1021/acsami.0c09446.
[17] B. Lee, H. Cho, K. T. Park, J. S. Kim, M. Park, H. Kim, Y. Hong, S. Chung, High-performance compliant thermoelectric generators with magnetically self-assembled soft heat conductors for self-powered wearable electronics, *Nature Communications*, 2020, **11**, 5948, doi: 10.1038/s41467-020-19756-z.
[18] R. Liu, Z. L. Wang, K. Fukuda, T. Someya, Flexible self-charging power sources, *Nature Reviews Materials*, 2022, **7**, 870-886, doi: 10.1038/s41578-022-00441-0.
[19] J. D. Ryan, A. Lund, A. I. Hofmann, R. Kroon, R. Sarabia Riquelme, M. C. Weisenberger, C. Müller, All-organic textile thermoelectrics with carbon-nanotube-coated n-type yarns, *ACS Applied Energy Materials*, 2018, **1**, 2934-2941, doi: 10.1021/acsaem.8b00617.
[20] Z. Liu, G. Chen, Advancing flexible thermoelectric devices with polymer composites, *Advanced Materials Technologies*, 2020, **5**, 2000049, doi: 10.1002/admt.202000049.
[21] Y. Liu, P. Liu, Q. Jiang, F. Jiang, J. Liu, G. Liu, C. Liu, Y. Du, J. Xu, Organic/inorganic hybrid for flexible thermoelectric fibers, *Chemical Engineering Journal*, 2021, **405**, 126510, doi: 10.1016/j.cej.2020.126510.
[22] L. Zhang, S. Lin, T. Hua, B. Huang, S. Liu, X. Tao, Fiber-based thermoelectric generators: materials, device structures, fabrication, characterization, and applications, *Advanced Energy Materials*, 2018, **8**, 1700524, doi: 10.1002/aenm.201700524.
[23] Y. Kim, A. Lund, H. Noh, A. I. Hofmann, M. Craighero, S. Darabi, S. Zokaei, J. I. Park, M.-H. Yoon, C. Müller, Robust PEDOT: PSS wet-spun fibers for thermoelectric textiles, *Macromolecular Materials and Engineering*, 2020, **305**, 1900749, doi: 10.1002/mame.201900749.
[24] A. J. Minnich, M. S. Dresselhaus, Z. F. Ren, G. Chen, Bulk nanostructured thermoelectric materials: current research and future prospects, *Energy & Environmental Science*, 2009, **2**, 466-479, doi: 10.1039/B822664B.
[25] J. He, T. M. Tritt, Advances in thermoelectric materials research: Looking back and moving forward, *Science*, 2017, **357**, eaak9997, doi: 10.1126/science.aak9997.
[26] D. Champier, Thermoelectric generators: a review of

applications, *Energy Conversion and Management*, 2017, **140**, 167-181, doi: 10.1016/j.enconman.2017.02.070.
[27] Y. Sargolzaeiaval, V. P. Ramesh, M. C. Ozturk, A comprehensive analytical model for thermoelectric body heat harvesting incorporating the impact of human metabolism and physical activity, *Applied Energy*, 2022, **324**, 119738, doi: 10.1016/j.apenergy.2022.119738.
[28] D. Beretta, N. Neophytou, J. M. Hodges, M. G. Kanatzidis, D. Narducci, M. Martin-Gonzalez, M. Beekman, B. Balke, G. Cerretti, W. Tremel, A. Zevalkink, A. I. Hofmann, C. Müller, B. Dörling, M. Campoy-Quiles, M. Caironi, Thermoelectrics: from history, a window to the future, *Materials Science and Engineering: R: Reports*, 2019, **138**, 100501, doi: 10.1016/j.mser.2018.09.001.
[29] X. Wang, P. Liu, Q. Jiang, W. Zhou, J. Xu, J. Liu, Y. Jia, X. Duan, Y. Liu, Y. Du, F. Jiang, Efficient DMSO-vapor annealing for enhancing thermoelectric performance of PEDOT: PSS-based aerogel, *ACS Applied Materials & Interfaces*, 2019, **11**, 2408-2417, doi: 10.1021/acsami.8b19168.
[30] N. Okada, K. Sato, M. Yokoo, E. Kodama, S. Kanehashi, T. Shimomura, Thermoelectric properties of poly(3-hexylthiophene) nanofiber aerogels with a giant seebeck coefficient, *ACS Applied Polymer Materials*, 2021, **3**, 455-463, doi: 10.1021/acsapm.0c01185.
[31] S. Han, N. U. H. Alvi, L. Granlöf, H. Granberg, M. Berggren, S. Fabiano, X. Crispin, A multiparameter pressure-temperature-humidity sensor based on mixed ionic-electronic cellulose aerogels, *Advanced Science*, 2019, **6**, 1802128, doi: 10.1002/advs.201802128.
[32] L. Liang, X. Wang, Z. Liu, G. Sun, G. Chen, Recent advances in organic, inorganic, and hybrid thermoelectric aerogels, *Chinese Physics B*, 2022, **31**, 027903, doi: 10.1088/1674-1056/ac2802.
[33] Z. Fan, Y. Zhang, L. Pan, J. Ouyang, Q. Zhang, Recent developments in flexible thermoelectrics: from materials to devices, *Renewable and Sustainable Energy Reviews*, 2021, **137**, 110448, doi: 10.1016/j.rser.2020.110448.
[34] S. Ortega, M. Ibáñez, Y. Liu, Y. Zhang, M. V. Kovalenko, D. Cadavid, A. Cabot, Bottom-up engineering of thermoelectric nanomaterials and devices from solution-processed nanoparticle building blocks, *Chemical Society Reviews*, 2017, **46**, 3510-3528, doi: 10.1039/C6CS00567E.
[35] N. Yanagishima, S. Kanehashi, H. Saito, K. Ogino, T. Shimomura, Thermoelectric properties of PEDOT: PSS aerogel secondary-doped in supercritical CO_2 atmosphere with low thermal conductivity, *Polymer*, 2020, **206**, 122912, doi: 10.1016/j.polymer.2020.122912.
[36] Y. Y. Hsieh, Y. Zhang, L. Zhang, Y. Fang, S. N. Kanakaraaj, J. H. Bahk, V. Shanov, High thermoelectric power-factor composites based on flexible three-dimensional graphene and polyaniline, *Nanoscale*, 2019, **11**, 6552-6560, doi: 10.1039/C8NR10537E.
[37] C. Yu, H. Kim, J. R. Youn, Y. S. Song, Enhancement of structural stability of graphene aerogel for thermal energy harvesting, *ACS Applied Energy Materials*, 2021, **4**, 11666-11674, doi: 10.1021/acsaem.1c02390.
[38] C. Yu, Y. S. Song, Analysis of thermoelectric energy harvesting with graphene aerogel-supported form-stable phase change materials, *Nanomaterials*, 2021, **11**, 2192, doi: 10.3390/nano11092192.
[39] X. Qi, T. Miao, C. Chi, G. Zhang, C. Zhang, Y. Du, M. An, W. G. Ma, X. Zhang, Ultralight PEDOT: PSS/graphene oxide composite aerogel sponges for electric power harvesting from thermal fluctuations and moist environment, *Nano Energy*, 2020, **77**, 105096, doi: 10.1016/j.nanoen.2020.105096.
[40] F. Jia, R. Wu, C. Liu, J. Lan, Y. H. Lin, X. Yang, High thermoelectric and flexible PEDOT/SWCNT/BC nanoporous films derived from aerogels, *ACS Sustainable Chemistry & Engineering*, 2019, **7**, 12591-12600, doi: 10.1021/acssuschemeng.9b02518.
[41] X. Sun, Y. Wei, J. Li, J. Zhao, L. Zhao, Q. Li, Ultralight conducting PEDOT: PSS/carbon nanotube aerogels doped with silver for thermoelectric materials, *Science China Materials*, 2017, **60**, 159-166, doi: 10.1007/s40843-016-5132-8.
[42] H. He, J. Liu, Y. Wang, Y. Zhao, Y. Qin, Z. Zhu, Z. Yu, J. Wang, An ultralight self-powered fire alarm e-textile based on conductive aerogel fiber with repeatable temperature monitoring performance used in firefighting clothing, *ACS Nano*, 2022, **16**, 2953-2967, doi: 10.1021/acsnano.1c10144.
[43] X. Z. Gao, F. L. Gao, J. Liu, Y. Li, P. Wan, Z. Z. Yu, X. Li, Self-powered resilient porous sensors with thermoelectric poly(3, 4-ethylenedioxythiophene): poly(styrenesulfonate) and carbon nanotubes for sensitive temperature and pressure dual-mode sensing, *ACS Applied Materials & Interfaces*, 2022, **14**, 43783-43791, doi: 10.1021/acsami.2c12892.
[44] Y. Wang, H. Mao, Y. Wang, P. Zhu, C. Liu, Y. Deng, 3D geometrically structured PANI/CNT-decorated polydimethylsiloxane active pressure and temperature dual-parameter sensors for man–machine interaction applications, *Journal of Materials Chemistry A*, 2020, **8**, 15167-15176, doi: 10.1039/D0TA05651K.
[45] X. He, Y. Hao, M. He, X. Qin, L. Wang, J. Yu, Stretchable thermoelectric-based self-powered dual-parameter sensors with decoupled temperature and strain sensing, *ACS Applied Materials & Interfaces*, 2021, **13**, 60498-60507, doi: 10.1021/acsami.1c20456.
[46] F. L. Gao, P. Min, X. Z. Gao, C. Li, T. Zhang, Z. Z. Yu, X. Li, Integrated temperature and pressure dual-mode sensors based on elastic PDMS foams decorated with thermoelectric PEDOT: PSS and carbon nanotubes for human energy harvesting and electronic-skin, *Journal of Materials Chemistry A*, 2022, **10**, 18256-18266, doi: 10.1039/D2TA04862K.
[47] D. Zhang, Y. Mao, P. Bai, Q. Li, W. He, H. Cui, F. Ye, C. Li, R. Ma, Y. Chen, Multifunctional superelastic graphene-based thermoelectric sponges for wearable and thermal management devices, *Nano Letters*, 2022, **22**, 3417-3424, doi: 10.1021/acs.nanolett.2c00696.
[48] H. Li, Z. Ding, Q. Zhou, J. Chen, Z. Liu, C. Du, L. Liang, G. Chen, Harness high-temperature thermal energy *via* elastic thermoelectric aerogels, *Nano-Micro Letters*, 2024, **16**, 151, doi:

10.1007/s40820-024-01370-z.
[49] Y. Shen, X. Han, P. Zhang, X. Chen, X. Yang, D. Liu, X. Yang, X. Zheng, H. Chen, K. Zhang, T. Zhang, Review on fiber-based thermoelectrics: materials, devices, and textiles, *Advanced Fiber Materials*, 2023, **5**, 1105-1140, doi: 10.1007/s42765-023-00267-7.
[50] F. D. Rosi, Thermoelectricity and thermoelectric power generation, *Solid-State Electronics*, 1968, **11**, 833-868, doi: 10.1016/0038-1101(68)90104-4.
[51] A. F. Ioffe, L. S. Stil'bans, E. K. Iordanishvili, T. S. Stavitskaya, A. Gelbtuch, G. Vineyard, *Semiconductor thermoelements and thermoelectric cooling, Physics Today*, 1959, **12**, 42, doi: 10.1063/1.3060810.
[52] N. Komatsu, Y. Ichinose, O. S. Dewey, L. W. Taylor, M. A. Trafford, Y. Yomogida, G. Wehmeyer, M. Pasquali, K. Yanagi, J. Kono, Macroscopic weavable fibers of carbon nanotubes with giant thermoelectric power factor, *Nature Communications*, 2021, **12**, 4931, doi: 10.1038/s41467-021-25208-z.
[53] G. J. Snyder, E. S. Toberer, Complex thermoelectric materials, *Nature Materials*, 2008, **7**, 105-114, doi: 10.1038/nmat2090.
[54] J. P. Heremans, V. Jovovic, E. S. Toberer, A. Saramat, K. Kurosaki, A. Charoenphakdee, S. Yamanaka, G. J. Snyder, Enhancement of thermoelectric efficiency in PbTe by distortion of the electronic density of states, *Science*, 2008, **321**, 554-557, doi: 10.1126/science.1159725.
[55] N. Toshima, Recent progress of organic and hybrid thermoelectric materials, *Synthetic Metals*, 2017, **225**, 3-21, doi: 10.1016/j.synthmet.2016.12.017.
[56] M. Cutler, J. F. Leavy, R. L. Fitzpatrick, Electronic transport in semimetallic cerium sulfide, *Physical Review*, 1964, **133**, A1143-A1152, doi: 10.1103/physrev.133.a1143.
[57] C. Gayner, K. K. Kar, Recent advances in thermoelectric materials, *Progress in Materials Science*, 2016, **83**, 330-382, doi: 10.1016/j.pmatsci.2016.07.002.
[58] R. P. Chasmar, R. Stratton, The thermoelectric figure of merit and its relation to thermoelectric generators, *Journal of Electronics and Control*, 1959, **7**, 52-72, doi: 10.1080/00207215908937186.
[59] X. L. Shi, J. Zou, Z. G. Chen, Advanced thermoelectric design: from materials and structures to devices, *Chemical Reviews*, 2020, **120**, 7399-7515, doi: 10.1021/acs.chemrev.0c00026.
[60] H. He, Y. Qin, Z. Zhu, Q. Jiang, S. Ouyang, Y. Wan, X. Qu, J. Xu, Z. Yu, Temperature-arousing self-powered fire warning E-textile based on p–n segment coaxial aerogel fibers for active fire protection in firefighting clothing, *Nano-Micro Letters*, 2023, **15**, 226, doi: 10.1007/s40820-023-01200-8.
[61] Z. Yu, Y. Wan, M. Zhou, M. H. Mia, S. Huo, L. Huang, J. Xu, Q. Jiang, Z. Zheng, X. Hu, H. He, Muscle-inspired anisotropic aramid nanofibers aerogel exhibiting high-efficiency thermoelectric conversion and precise temperature monitoring for firefighting clothing, *Nano-Micro Letters*, 2025, **17**, 214, doi: 10.1007/s40820-025-01728-x.
[62] S. Liu, D. Wu, S. N. University, M. Kong, W. Wang, S. T. University, L. Xie, G. B. University, J. He, High-entropy thermoelectric materials: advances, challenges, and future opportunities, *ACS Energy Letters*, 2025, **10**, 925-934, doi: 10.1021/acsenergylett.4c03369.
[63] Q. Cheng, Z. Sheng, Y. Ding, Y. Li, X. Zhang, 3D printed colloidal aerogels: Principle, process, performance, and perspective, *Progress in Materials Science*, 2025, **152**, 101456, doi: 10.1016/j.pmatsci.2025.101456.
[64] X. Hou, J. Chen, Z. Chen, D. Yu, S. Zhu, T. Liu, L. Chen, Flexible aerogel materials: a review on revolutionary flexibility strategies and the multifunctional applications, *ACS Nano*, 2024, **18**, 11525-11559, doi: 10.1021/acsnano.4c00347.
[65] Y. Chen, M. Shafiq, M. Liu, Y. Morsi, X. Mo, Advanced fabrication for electrospun three-dimensional nanofiber aerogels and scaffolds, *Bioactive Materials*, 2020, **5**, 963-979, doi: 10.1016/j.bioactmat.2020.06.023.
[66] X. Guo, Y. Zhang, J. Li, Y. Hao, H. Ke, P. Lv, Q. Wei, Wet spinning technology for aerogel fiber: pioneering the frontier of high-performance and multifunctional materials, *Advanced Fiber Materials*, 2024, **6**, 1669-1709, doi: 10.1007/s42765-024-00440-6.
[67] J. Zhou, Y.-L. Hsieh, Nanocellulose aerogel-based porous coaxial fibers for thermal insulation, *Nano Energy*, 2020, **68**, 104305, doi: 10.1016/j.nanoen.2019.104305.
[68] Z. Xu, Y. Liu, Q. Xin, J. Dai, J. Yu, L. Cheng, Y. T. Liu, B. Ding, Ceramic meta-aerogel with thermal superinsulation up to 1700 °C constructed by self-crosslinked nanofibrous network *via* reaction electrospinning, *Advanced Materials*, 2024, **36**, e2401299, doi: 10.1002/adma.202401299.
[69] Q. Jiang, Y. Wan, Y. Qin, X. Qu, M. Zhou, S. Huo, X. Wang, Z. Yu, H. He, Durable and wearable self-powered temperature sensor based on self-healing thermoelectric fiber by coaxial wet spinning strategy for fire safety of firefighting clothing, *Advanced Fiber Materials*, 2024, **6**, 1387-1401, doi: 10.1007/s42765-024-00416-6.
[70] H. He, Y. Qin, J. Liu, Y. Wang, J. Wang, Y. Zhao, Z. Zhu, Q. Jiang, Y. Wan, X. Qu, Z. Yu, A wearable self-powered fire warning e-textile enabled by aramid nanofibers/MXene/silver nanowires aerogel fiber for fire protection used in firefighting clothing, *Chemical Engineering Journal*, 2023, **460**, 141661, doi: 10.1016/j.cej.2023.141661.
[71] E. C. Bate-Smith, Applications of freeze-drying techniques, *Nature*, 1965, **206**, 538-539, doi: 10.1038/206538a0.
[72] H. Zhu, X. Yang, E. D. Cranston, S. Zhu, Flexible and porous nanocellulose aerogels with high loadings of metal-organic-framework particles for separations applications, *Advanced Materials*, 2016, **28**, 7652-7657, doi: 10.1002/adma.201601351.
[73] F. Xu, J. Xu, H. Xu, Y. Lu, H. Yang, Z. Tang, Z. Lu, R. Fu, D. Wu, Fabrication of novel powdery carbon aerogels with high surface areas for superior energy storage, *Energy Storage Materials*, 2017, **7**, 8-16, doi: 10.1016/j.ensm.2016.11.002.
[74] W. Song, X. Pan, X. Wang, H. Wang, J. Li, D. Li, X. Ma, F. Yin, Load-bearing structure inspired cellulose-based aerogel with high resilience and water tolerance, *Advanced Functional Materials*, 2025, **35**, 2415937, doi: 10.1002/adfm.202415937.

[75] J. Ren, X. Huang, R. Han, G. Chen, Q. Li, Z. Zhou, Avian bone-inspired super fatigue resistant MXene-based aerogels with human-like tactile perception for multilevel information encryption assisted by machine learning, *Advanced Functional Materials*, 2024, **34**, 2403091, doi: 10.1002/adfm.202403091.
[76] H. Tetik, J. Orangi, G. Yang, K. Zhao, S. B. Mujib, G. Singh, M. Beidaghi, D. Lin, 3D printed MXene aerogels with truly 3D macrostructure and highly engineered microstructure for enhanced electrical and electrochemical performance, *Advanced Materials*, 2022, **34**, e2104980, doi: 10.1002/adma.202104980.
[77] Q. Chen, J. Shen, D. Estevez, Y. Chen, Z. Zhu, J. Yin, F. Qin, Ultraprecise 3D printed graphene aerogel microlattices on tape for micro sensors and E-skin, *Advanced Functional Materials*, 2023, **33**, 2302545, doi: 10.1002/adfm.202302545.
[78] Y. Li, D. Yang, Z. Wu, F. L. Gao, X. Z. Gao, H. Y. Zhao, X. Li, Z. Z. Yu, Self-adhesive, self-healing, biocompatible and conductive polyacrylamide nanocomposite hydrogels for reliable strain and pressure sensors, *Nano Energy*, 2023, **109**, 108324, doi: 10.1016/j.nanoen.2023.108324.
[79] H. E. Baysal, T. Y. Yu, V. Naenen, S. De Smedt, D. Hiz, B. Zhang, H. Xia, I. Florenciano, M. Rosenthal, R. Cardinaels, F. Molina-Lopez, Omnidirectional 3D printing of PEDOT: PSS aerogels with tunable electromechanical performance: a playground for unconventional stretchable interconnects and thermoelectrics, *Advanced Science*, 2025, **12**, 2412491, doi: 10.1002/advs.202412491.
[80] T. Li, Y. Huang, J. X. M. Chen, Y. C. Sun, O. Aghababaei, Z. Saadatnia, H. E. Naguib, 3D printing of conductive polymer aerogel thermoelectric generator with tertiary doping, *Nano Energy*, 2023, **117**, 108909, doi: 10.1016/j.nanoen.2023.108909.
[81] X. Fu, L. Si, Z. Zhang, T. Yang, Q. Feng, J. Song, S. Zhu, D. Ye, Gradient all-nanostructured aerogel fibers for enhanced thermal insulation and mechanical properties, *Nature Communications*, 2025, **16**, 2357, doi: 10.1038/s41467-025-57646-4.
[82] G. Wei, J. Zhang, M. Usuelli, X. Zhang, B. Liu, R. Mezzenga, Biomass vs inorganic and plastic-based aerogels: structural design, functional tailoring, resource-efficient applications and sustainability analysis, *Progress in Materials Science*, 2022, **125**, 100915, doi: 10.1016/j.pmatsci.2021.100915.
[83] X. C. Lin, S. L. Li, W. X. Li, Z. H. Wang, J. Y. Zhang, B. W. Liu, T. Fu, H. B. Zhao, Y. Z. Wang, Thermo-responsive self-ceramifiable robust aerogel with exceptional strengthening and thermal insulating performance at ultrahigh temperatures, *Advanced Functional Materials*, 2023, **33**, 2214913, doi: 10.1002/adfm.202214913.
[84] S. Takeshita, S. Mine, T. Ono, Data-driven review on aerogels and polymeric aerogels, *Angewandte Chemie (International Ed)*, 2025, **64**, e202504250, doi: 10.1002/anie.202504250.
[85] L. Tian, F. L. Gao, Y. X. Li, Z. Y. Yang, X. Xu, Z. Z. Yu, J. Shang, R. W. Li, X. Li, High-performance bimodal temperature/pressure tactile sensor based on lamellar CNT/MXene/cellulose nanofibers aerogel with enhanced multifunctionality, *Advanced Functional Materials*, 2025, **35**, 2418988, doi: 10.1002/adfm.202418988.
[86] X. He, M. Liu, J. Cai, Z. Li, Z. Teng, Y. Hao, Y. Cui, J. Yu, L. Wang, X. Qin, Waste cotton-derived fiber-based thermoelectric aerogel for wearable and self-powered temperature–compression strain dual-parameter sensing, *Engineering*, 2024, **39**, 235-243, doi: 10.1016/j.eng.2024.01.015.
[87] S. Chen, S. Fan, Z. Qiao, Z. Wu, B. Lin, Z. Li, M. A. Riegler, M. Y. H. Wong, A. Opheim, O. Korostynska, K. M. Nielsen, T. Glott, A. C. T. Martinsen, V. H. Telle-Hansen, C. T. Lim, Transforming healthcare: intelligent wearable sensors empowered by smart materials and artificial intelligence, *Advanced Materials*, 2025, **37**, 2500412, doi: 10.1002/adma.202500412.
[88] M. Gao, P. Wang, L. Jiang, B. Wang, Y. Yao, S. Liu, D. Chu, W. Cheng, Y. Lu, Power generation for wearable systems, *Energy & Environmental Science*, 2021, **14**, 2114-2157, doi: 10.1039/D0EE03911J.
[89] P. Bhatnagar, S. H. Zaferani, N. Rafiefard, B. Baraeinejad, A. R. Vazifeh, R. Mohammadpour, R. Ghomashchi, H. Dillersberger, D. Tham, D. Vashaee, Advancing personalized healthcare and entertainment: progress in energy harvesting materials and techniques of self-powered wearable devices, *Progress in Materials Science*, 2023, **139**, 101184, doi: 10.1016/j.pmatsci.2023.101184.
[90] W. Tang, Q. Sun, Z. L. Wang, Self-powered sensing in wearable Electronics—A paradigm shift technology, *Chemical Reviews*, 2023, **123**, 12105-12134, doi: 10.1021/acs.chemrev.3c00305.
[91] Y. Yu, X. Liao, W. Feng, Recent development of elastomer-based smart sensing materials and structures, *Advanced Composites and Hybrid Materials*, 2025, **8**, 138, doi: 10.1007/s42114-024-01168-y.
[92] L. Han, K. Li, Z. Wang, W. Men, X. Wu, X. Sun, J. Zhang, J. Cheng, 3D printing flexible wearable electronics with diversified environmentally adaptive for biomechanical energy harvesting and personal electromagnetic safety, *Advanced Functional Materials*, 2025, 2424743, doi: 10.1002/adfm.202424743.
[93] Y. Wang, X. Feng, X. Chen, Autonomous bioelectronic devices based on silk fibroin, *Advanced Materials*, 2025, **37**, e2500073, doi: 10.1002/adma.202500073.
[94] G. Zhou, X. Qu, L. Tong, B. Wei, Y. Sun, Z. Mou, Q. Zhang, S. Ramakrishna, Q. Meng, Preparation and performance of Zr-Si based ultra thermal-insulating ceramic aerogels inspired by alpaca wool under extreme temperatures, *Chemical Engineering Journal*, 2025, **511**, 162033, doi: 10.1016/j.cej.2025.162033.
[95] Z. Yu, Y. Wan, Y. Qin, Q. jiang, J.-P. Guan, X.-W. Cheng, X. Wang, S. Ouyang, X. Qu, Z. Zhu, J. Wang, H. He, High fire safety thermal protective composite aerogel with efficient thermal insulation and reversible fire warning performance for firefighting clothing, *Chemical Engineering Journal*, 2023, **477**, 147187, doi: 10.1016/j.cej.2023.147187.
[96] Y. Wang, J. Liu, Y. Zhao, Y. Qin, Z. Zhu, Z. Yu, H. He, Temperature-triggered fire warning PEG@wood powder/carbon nanotube/calcium alginate composite aerogel and the application

for firefighting clothing, *Composites Part B: Engineering*, 2022, **247**, 110348, doi: 10.1016/j.compositesb.2022.110348.
[97] T. Sun, L. Wang, W. Jiang, Pushing thermoelectric generators toward energy harvesting from the human body: Challenges and strategies, *Materials Today*, 2022, **57**, 121-145, doi: 10.1016/j.mattod.2022.06.001.
[98] W. Ding, X. Shen, M. Jin, Y. Hu, Z. Chen, E. Meng, J. Luo, W. Li, Y. Pei, Robust bendable thermoelectric generators enabled by elasticity strengthening, *Nature Communications*, 2024, **15**, 9767, doi: 10.1038/s41467-024-54084-6.
[99] L. Miao, S. Zhu, C. Liu, J. Gao, Z. Zhang, Y. Peng, J. L. Chen, Y. Gao, J. Liang, T. Mori, Comfortable wearable thermoelectric generator with high output power, *Nature Communications*, 2024, **15**, 8516, doi: 10.1038/s41467-024-52841-1.
[100] S. Masoumi, S. O'Shaughnessy, A. Pakdel, Organic-based flexible thermoelectric generators: from materials to devices, *Nano Energy*, 2022, **92**, 106774, doi: 10.1016/j.nanoen.2021.106774.
[101] B. Xu, Y. Tian, Breaking a bottleneck for thermoelectric generators, *Science*, 2023, **382**, 882-883, doi: 10.1126/science.adl2157.
[102] M. Feng, S. Lv, J. Deng, Y. Guo, Y. Wu, G. Shi, M. Zhang, An overview of environmental energy harvesting by thermoelectric generators, *Renewable and Sustainable Energy Reviews*, 2023, **187**, 113723, doi: 10.1016/j.rser.2023.113723.
[103] S. El Oualid, I. Kogut, M. Benyahia, E. Geczi, U. Kruck, F. Kosior, P. Masschelein, C. Candolfi, A. Dauscher, J. D. Koenig, A. Jacquot, T. Caillat, E. Alleno, B. Lenoir, Thermoelectric generators: high power density thermoelectric generators with skutterudites (adv. energy mater. 19/2021), *Advanced Energy Materials*, 2021, **11**, 2170073, doi: 10.1002/aenm.202170073.